THE FASEB JOURNAL • RESEARCH • www.fasebj.org

Pth4, an ancient parathyroid hormone lost in eutherian mammals, reveals a new brain-to-bone signaling pathway

Paula Suarez-Bregua,* Eva Torres-Nuñez,* Ankur Saxena,[†,‡] Pedro Guerreiro,[§] Ingo Braasch,[¶] David A. Prober,[†] Paloma Moran,[‖] Jose Miguel Cerda-Reverter,[#] Shao Jun Du, Fatima Adrio,[††] Deborah M. Power,[§] Adelino V. M. Canario,[§] John H. Postlethwait,[¶] Marianne E. Bronner,[†] Cristian Cañestro,[‡‡] and Josep Rotllant*[,1]**

*Institute of Marine Research, Spanish National Research Council (IIM–CSIC), Vigo, Spain; [†]California Institute of Technology, Pasadena, California, USA; [‡]Department of Biological Sciences, University of Illinois, Chicago, Illinois, USA; [§]Center of Marine Sciences (CCMAR), University of Algarve, Faro, Portugal; [¶]Institute of Neuroscience, University of Oregon, Eugene, Oregon, USA; [‖]Department of Biochemistry, Genetics, and Immunology, University of Vigo, Vigo, Spain; [#]Institute of Aquaculture Torre de La Sal (IATS–CSIC), Castellón, Spain; **Department of Molecular and Cellular Biology, University of Maryland, Baltimore, Maryland, USA; [††]Department of Cell Biology, University of Santiago de Compostela, Santiago de Compostela Spain; and [‡‡]Department de Genètica, Microbiologia i Estadística, Institut de Recerca de la Biodiversitat (IRBio), Universitat de Barcelona, Barcelona, Spain

ABSTRACT: Regulation of bone development, growth, and remodeling traditionally has been thought to depend on endocrine and autocrine/paracrine modulators. Recently, however, brain-derived signals have emerged as key regulators of bone metabolism, although their mechanisms of action have been poorly understood. We reveal the existence of an ancient parathyroid hormone (Pth)4 in zebrafish that was secondarily lost in the eutherian mammals' lineage, including humans, and that is specifically expressed in neurons of the hypothalamus and appears to be a central neural regulator of bone development and mineral homeostasis. Transgenic fish lines enabled mapping of axonal projections leading from the hypothalamus to the brainstem and spinal cord. Targeted laser ablation demonstrated an essential role for of *pth4*-expressing neurons in larval bone mineralization. Moreover, we show that Runx2 is a direct regulator of *pth4* expression and that Pth4 can activate cAMP signaling mediated by Pth receptors. Finally, gain-of-function experiments show that Pth4 can alter calcium/phosphorus levels and affect expression of genes involved in phosphate homeostasis. Based on our discovery and characterization of Pth4, we propose a model for evolution of bone homeostasis in the context of the vertebrate transition from an aquatic to a terrestrial lifestyle.—Suarez-Bregua, P., Torres-Nuñez, E., Saxena, A., Guerreiro, P., Braasch, I., Prober, D. A., Moran, P., Cerda-Reverter, J. M., Du, S. J., Adrio, F., Power, D. M., Canario, A. V. M., Postlethwait, J. H., Bronner, M E., Cañestro, C., Rotllant, J. Pth4, an ancient parathyroid hormone lost in eutherian mammals, reveals a new brain-to-bone signaling pathway. FASEB J. 31, 569–583 (2017). www.fasebj.org

KEY WORDS: runx · phosphate · calcium · hypothalamus · fgf23

Bone is a highly specialized vertebrate-specific tissue that functions as a supporting structure characterized by its resistance, stiffness, and high capacity for regeneration and repair. To achieve these characteristics, bones are first shaped during early life and then constantly remodeled throughout adulthood. Bone remodeling is a lifelong process that relies on complex regulatory mechanisms to achieve proper rates of growth and differentiation.

ABBREVIATIONS: *Actb1*, actin-β1; BLAST, Basic Local Alignment Search Tool; BMD, bone mineral density; dpf, days post fertilization; *eef1a1/1*, elongation factor 1-α1 like 1; eGFP, enhanced green fluorescent protein; *entpd5*, ectonucleoside triphosphate diphosphohydrolase 5; *fgf23*, fibroblast growth factor 23; FISH, fluorescence ISH; HEK, human embryonic kidney; hpf, hours post fertilization; *hrct*, hypocretin gene; IBMX, 3-isobutyl-1-methylxantine; ISH, *in situ* hybridization; *npt2a*, sodium-phosphate cotransporter type IIa; MO, morpholino oligonucleotide; OGM, ohnologs gone missing; PFA, paraformaldehyde; *phex*, endopeptidase on the X chromosome; pl, primary lamella; *pth1r*, parathyroid hormone 1 receptor; PTH, parathyroid hormone; PTHLH, parathyroid hormone like-hormone; qPCR, quantitative PCR; *slc34a1a*, solute carrier family 34 sodium/phosphate cotransporter 1a; RACE, rapid amplification of cDNA ends; *stc1l*, stanniocalcin-1-like; TFBS, transcription factor binding site; Tg, transgenic; TPp, periventricular nucleus of posterior tuberculum; TSS, translation start site; TU, Tübingen; vBMD, volumetric bone mineral density; VGD, vertebrate genome duplication; VOI, volume of interest; WGD, whole-genome duplication; WISH, whole-mount ISH; WT, wild-type

[1] Correspondence: Institute of Marine Research, Spanish National Research Council (IIM-CSIC), Vigo, Spain. E-mail: rotllant@iim.csic.es

doi: 10.1096/fj.201600815R
This article includes supplemental data. Please visit *http://www.fasebj.org* to obtain this information.

Vertebrates regulate bone mineralization and remodeling at 3 main levels: delivery of systemic hormones [*e.g.*, parathyroid hormone (PTH) peptides and calcitonin], turnover of bone cells (*e.g.*, osteoblasts, osteoclasts, and osteocytes), and auto-regulatory feedback loops mediated by cell-signaling products [*e.g.*, fibroblast growth factor (FGF)-23, and ectonucleoside triphosphate diphosphohydrolase (ENTPD)-5)] (1, 2). In addition to the complex network of endocrine, autocrine, and paracrine hormone signals that tightly regulate bone mineral metabolism, recent studies suggest that the brain is a pivotal regulator of bone homeostasis through 3 distinct pathways. The first pathway includes hormonal signals that arise from neuroendocrine neurons of the hypothalamus and are subsequently processed in the pituitary [*e.g.*, leptin, proopiomelacortin-derived peptides, gonadotrophin hormone releasing hormone (GnRH), and thyrotropin releasing hormone] (3–6). The second pathway consists of neuronal factors released by the hypothalamus and distributed through the bloodstream [*e.g.*, cocaine-and amphetamine-regulated transcript, neuropeptide Y, agouti-related peptide, and brain-derived neurotrophic factor (6)]. The third pathway consists of efferent neuronal signaling that regulates the sympathetic and parasympathetic nervous systems (7). The high interconnectivity of the hypothalamus in the brain makes this structure one of the most powerful regulatory regions of the body, integrating signals not only from peripheral tissues but also from other areas within the brain itself. Understanding the novel regulatory axes between brain and bone cells is therefore critical for a better understanding of bone biology.

Using a reverse genetic approach, we identified a new brain-to-bone pathway involving efferent neural signals from the hypothalamus to receptors on bone cells controlling skeletal mineralization and phosphate homeostasis in teleosts. The key factor of this new brain-to-bone pathway appears to be an ancestral PTH family member that has been conserved in ray-finned fish, lobe-finned fish, and noneutherian mammals, but surprisingly has been lost in eutherian vertebrates.

The PTH family of peptides plays a central role in phosphocalcic homeostasis, bone remodeling, and embryonic skeleton development in vertebrates (8–11). In tetrapods, PTH is synthesized by the parathyroid glands (PTGs) and plays a pivotal role in bone turnover by regulating the metabolism of calcium and phosphate. Fish have homologs of PTH and PTH-like peptides (*i.e.*, PTH2 and PTHLH). In contrast to tetrapods, however, none of these fish PTH peptides seems to regulate calcium and phosphate metabolism during bone turnover (10, 12). These taxon-specific differences are likely related to the transition from aquatic to terrestrial environments that occurred during the evolution of tetrapods, in which new mechanisms for controlling bone homeostasis became associated with the evolution of the PTH family and possibly facilitated the transition from an aquatic to terrestrial lifestyle, which was accompanied by greater stress on skeletal elements.

We describe experiments that demonstrate that the novel PTH family member Pth4 is unique to noneutherian vertebrates and acts as a neuropeptide produced by a specific subset of neurons located in the dorsal part of the periventricular hypothalamus, with axonal projections leading from the hypothalamus to the brainstem and spinal cord. Loss- and gain-of-function experiments provided functional evidence that Pth4 is a powerful regulator of bone mineral accrual acting through phosphate homeostasis. We also provide evidence that Runx2 directly regulates Pth4 upstream and downstream, all Pth receptors facilitate activating cAMP signaling. Finally, in light of our new data and a reexamination of the evolution of the PTH family in fish and tetrapods, we propose a model describing the evolution of Pth signaling related to bone remodeling in the context of vertebrate evolution.

MATERIALS AND METHODS

Fish

Fish (zebrafish, *Danio rerio*) were cultured as previously described (13) and staged by hours post fertilization (hpf) or days post fertilization (dpf), according to standard criteria (14). Experiments were performed with a Tübingen (TU)-wild-type (WT) strain [(TU), Nüsslein-Volhard Laboratory, Max Planck Institute, Tübingen, Germany]. For some experiments, embryo medium was supplemented with 0.003% (w/v) 2-phenylthiourea to inhibit embryo pigmentation (13). For histology, dechorionated embryos were fixed overnight at 4°C in 4% paraformaldehyde (PFA) in 1× PBS, washed in PBS, and stored at 4°C in 1× PBS for confocal imaging or dehydrated through a methanol series and stored at −20°C in 100% methanol for *in situ* hybridization (ISH). Ethics approval (ref: AGL2014-52473R) for all studies was obtained from the Institutional Animal Care and Use Committee of the IIM-CSIC Institute in accordance with the National Advisory Committee for Laboratory Animal Research Guidelines licensed by the Spanish Authority (RD53/2013) and conformed to European animal directive (2010/63/UE) for the protection of experimental animals.

DNA cloning

The putative zebrafish *pth4* gene was identified by searching the zebrafish genome database, Zv9, with translated Basic Local Alignment Search Tool [tBLASTn; National Institutes of Health, National Center for Biotechnology Information (NCBI), Bethesda, MD, USA; *http://blast.ncbi.nlm.nih.gov/Blast.cgi*] using the previously identified sequence of zebrafish Pth1a, Pth1b, Pth2 (Tip39), Pthlha, and Pthlhb paralogs (accession nos.: NM_212950, NM_212949, NP_991140, NP_001019798.2, and NP_001036789.1, respectively). Full-length cDNA was isolated by using sequence-specific primers (Supplemental Table S2) in 5′ and 3′ Smart RACE (rapid amplification of cDNA ends) cDNA amplification kit (TaKaRa, Mountain View, CA, USA), and sequenced by Sanger method. The zebrafish *pth4* gene sequence has been submitted to the European Molecular Biology Laboratory (EMBL)/NCBI GenBank database (accession no. KT182088; *https://www.ncbi.nlm.nih.gov/genbank*).

Phylogenetic analysis and comparative genomic of conserved synteny

Multiple sequence alignment was made by the Muscle pctid-log algorithm, corrected manually for inconsistencies and trimmed to decrease the total number of gaps (Supplemental Fig. S3). Phylogenetic analysis was inferred by maximum likelihood using PhyML 3.0 subjected to LG substitution model, a bionj starting tree improved by NNI, and computing aLRT SH-like

branch support (15). Analyses of conserved synteny were performed using automated pipeline tools of the Synteny Database variant Ens61 (16). Dot-plots represent the chromosomal distribution of human ohnologs [a special type of paralogs resulting by whole-genome duplication (WGD) (17)] of gene neighbors of the PTH family. The first 20 Mb of human chromosome 11 (Hsa11), which includes the human *PTH* gene, were analyzed taking the genomes of the urochordate *Ciona intestinalis* and the cephalochordate *Branchiostoma floridae* as outgroups for the identification of ohnologs resulting from the first and second rounds of vertebrate genome duplication [VGD1 and -2; for details see Cañestro *et al*. (18)]. Clusters in the Synteny Database were obtained by coupling results from the reciprocal best-hit BLAST pipeline with the use of a 50- or 25-gene sliding window analysis that links orthologous chromosome segments of 2 species by conserved synteny (16). The Synteny Database is especially useful to provide evidence of ohnologs gone missing (OGM) by uncovering the putative chromosomal region that still preserves paralogous syntenic conservation, but has lost a certain ohnolog of interest (18, 19).

Real-time quantitative PCR

Temporal expression of *pth4* was determined by real-time PCR. Total RNA was isolated at 0, 3, 6, 9, 12, and 14 hpf and 1, 2, 3, 4, 5, and 6 dpf, using Trizol reagent (Thermo Fisher Scientific) and first-strand cDNA was synthesized according to the Maxima First Strand cDNA Synthesis Kit (Thermo Fisher Scientific) protocol starting with 500 ng of total RNA. The partial sequence of *pth4* was amplified by using DreamTaq DNA Polymerase (Thermo Fisher Scientific) and specific primers (Supplemental Table S1). 18S ribosomal cDNA amplification was used as a positive control. Gene markers of phosphocalcic metabolism were analyzed by real-time quantitative PCR (qPCR). Total RNA from TU-WT and Tg(Xla.Eef1a1:pth4)iim010 adult male zebrafish (n = 6 per group) was extracted and reverse-transcribed as described above with specific primers (Supplemental Table S1). Each sample was amplified in triplicate containing 12.5 μl of Maxima SYBR Green/ROX qPCR Master Mix (2×) (Thermo Fisher Scientific), 0.5 μl 0.2 μM of each primer, 10.5 μl nuclease-free water, and 1 μl cDNA template. Real-time qPCR reactions were analyzed on a 7500 Fast Real-Time PCR System (Thermo Fisher Scientific) with the following cycling conditions: initial denaturation at 95°C for 10 min, followed by 40 cycles at 95°C for 15 s and 60°C for 1 min. Gene expression was assessed in 2 independent experiments using the efficiency calibrated method (20), and relative mRNA expression levels were normalized to *18S*, eukaryotic translation elongation factor 1-α1-like 1 (*eef1a1l1*) and actin β1(*actb1*).

Whole-mount ISH and immunohistochemistry

Whole-mount ISH (WISH) was performed using digoxigenin-labeled antisense riboprobes (21). Antisense and sense riboprobes were made from linearized full-length zebrafish *pth4*, *pth2*, and *pth1ra* cDNA. For plastic sections, embryos with ISH staining were fixed, dehydrated, Epon embedded, cut into 4 μm rostrocaudal transverse sections, mounted with Eukitt (EMS, Hatfield, PA, USA) as previously described (13) and imaged with a DM2500 microscope (Leica, Wetzlar, Germany). ISH of adult zebrafish sections (360 dpf) followed published methods (22). Samples were fixed in 4% PFA and 0.1 M phosphate buffer, for 2 d at 4°C, dehydrated and embedded in Paraplast (Sherwood, St. Louis, MO, USA). Serial 10-μm rostrocaudal transverse sections were cut on a rotary microtome. Sections were mounted on 3-aminopropyltriethoxylane-treated slides, air-dried at room temperature overnight, and stored at 4°C in dry conditions and used for hybridization within 1 month. Double labeling of enhanced green fluorescent protein (eGFP) immunofluorescence and fluorescence ISH (FISH) was performed in 3-dpf Tg(pth4:eGFP)iim07 zebrafish embryos. A sheep anti-DIG-POD antibody (Roche Diagnostics, Indianapolis, IN, USA) was used and *pth4* probe labeling was detected by tyramide signal amplification (TSA Plus Cyanine 3 and Fluorescein system; PerkinElmer, Waltham, MA, USA). Expression of eGFP was visualized with a mouse anti-eGFP primary antibody (Roche Diagnostics) followed by a horse anti-mouse fluorescein-conjugated secondary antibody (Vector Laboratories, Burlingame, CA, USA). For cryostat sectioning, Tg(pth4:eGFP)iim07 adult fish were fixed in 4% paraformaldehyde overnight at 4°C, washed with PBS, transferred to 15% sucrose, followed by 30% sucrose, and then embedded and frozen in optimal cutting temperature medium. Cross-cryosections of 25 μm thickness were collected on polylysine slides (Thermo Fisher Scientific) and allowed to dry. Slides were washed in PBS, mounted in Vectashield, and imaged on a TCS SP5 (Leica) confocal microscope. Cartilage–bone staining was performed with a 2-color acid-free stain (21).

cAMP based β- galactosidase reporter gene assay

To demonstrate whether Pth4 was able to bind and signal through PTH receptors, we performed cAMP-based β-galactosidase reporter gene assays. We amplified the predicted region for the *pth4* mature peptide and full coding regions of the *pth1ra*, *pth2r* [splice variant *pth2r* (23) and *pth1rb*; previous names: *pth1r*, *pth2r*, and *pth3r*, respectively] from cDNA template by PCR using Pfu Ultra II HS DNA polymerase (Agilent Technologies, Santa Clara, CA, USA) and specific primers (Supplemental Table S2), and cloned the fragments into pSC-B-amp/kan (Agilent Technologies). Inserts were subcloned into pcDNA3 (Thermo Fisher Scientific). All constructs were verified by sequencing both DNA strands. Signaling *via* cAMP was assessed using a human embryonic (HEK)-293 cell clone (Clon-Q) that stably expresses β-galactosidase under the control of human vasoactive intestinal peptide promoter placed downstream of tandem repetitions of cAMP response elements (24). Cells were transfected with 1.5 μg for pcDNA3-*pth4* or 1 μg of pcDNA3-*pth1ra*, pcDNA3-*pthr2*, or pcDNA3-*pth1rb*, using Lipofectamine LIX and Plus Reagent according to the manufacturer's protocol (Thermo Fisher Scientific). A construct carrying the *eGFP* gene under the control of a cytomegalovirus constitutive promoter was also transfected to standardize transfection levels. After 24 h, transfection was assessed by analyzing the eGFP fluorescence and transfected cells with receptors were plated in 96-well plates (50,000 cells/well). Cells expressing Pth4 mature peptides were rinsed with PBS and lysed by thermal shock, spin dried at 1100 relative centrifugal force (rcf) for 5 min at 22°C, and the supernatant collected. Recombinant cells expressing each receptor were stimulated for 6 h at 37°C with 100 μl of decreasing concentrations (1:2, 1:4, 1:8, 1:16, 1:32, 1:64, and 1:128 dilutions) of peptide solution from cellular lysates containing 0.1 mM of 3-isobutyl-1-methylxantine (IBMX; Sigma-Aldrich, St. Louis, MO, USA), a phosphodiesterase inhibitor that prevent enzymatic degradation of cAMP. As positive controls, we used 0.001 mM forskolin and 10^{-6} M human (h) PTH (Sigma-Aldrich) (25). Measurements were normalized for protein content, which was determined using the BCA protein assay kit (Thermo Fisher Scientific). Negative controls were performed using cells transfected with empty pcDNA3 vector (Thermo Fisher Scientific). All experiments were performed in triplicate. Data are presented as a percentage of negative control values. cAMP based β-galactosidase reporter gene assays were performed, as previously described (26, 27).

Transgene construction and microinjection

To ectopically express *pth4*, 3 independent transgenic (Tg) zebrafish lines were generated with the *Tol2* transposon system: Tg(Xla.Eef1a1:pth4)iim010, Tg(Xla.Eef1a1:pth4)iim011, and Tg(Xla.

Eef1a1:pth4)iim012. The *Tol2* vector was kindly provided by Koichi Kawakami, National Institute of Genetics, Mishimi, Japan (28). The *pth4* PCR product was subcloned into pGEM-T easy vector (Promega, Madison, WI, USA) with *Bam*HI and *Not*I restriction sites. pGEM-T-*pth4* was digested with *Bam*HI and *Not*I and subcloned into *pT2AL200R150G* cut with the same restriction enzymes. The Tol2-transposon-based vector *pT2AL200R150G* contained an *eGFP* gene under the control of constitutive promoter of the elongation factor 1-α (Eef1a1). We replaced the *eGFP* gene with the *pth4* gene. To generate *pth4* reporter lines, zebrafish *pth4* promoter sequences containing 2 and 1 kb upstream to the translation starting site (TSS) of the *pth4* gene (GenBank accession no. CU856139.10) for the *Tol2* transposon constructs used in this study were amplified from 6 dpf zebrafish genomic DNA with KOD Xtrem Hot Start DNA Polymerase Platinum (71975; Novagen, Madison, WI, USA) and specific primers (Supplemental Table S3). The PCR products (2394 and 890 bp) were diluted 1:10, and 1 μl was ligated into 1 μl of P-ENTR/D-TOPO Cloning Kit (Thermo Fisher Scientific) and transformed according to the manufacturer's instructions. Both promoter sequences were then ligated by LR Clonase into the destination vector *pToleGFPDest* (274; Lawson Lab, Malvern, PA, USA) containing the *eGFP* sequence downstream, and sequenced. Construct P1 (*1kb-pth4-Tol2-eGFP*) contained 873 nucleotides upstream to the TSS of the *pth4* gene. Construct P2 (*2kb-pth4-Tol2-eGFP*) contained 2377 nucleotides upstream to the TSS of the *pth4* gene. Three P2 independent Tg zebrafish lines Tg(pth4:eGFP)iim07, Tg(pth4:eGFP)iim08, and Tg(pth4:eGFP)iim09 were generated. To study the regulatory region of *pth4*, potentially *cis*-acting transcription factor binding sites (TFBSs) located in the zebrafish *pth4* promoter sequence were identified with MatInspector software (29). Deletion and substitution mutations were created as has been described (30) or by using the QuickChange Site-Directed Mutagenesis Kit (Stratagene, La Jolla, CA, USA). The resulting clones were tested though restriction analysis and confirmed by sequencing. *All Tol2* constructs (Supplemental Tables S3, S4) were dissolved in distilled RNAase-free water to a final concentration of 50 μg/ml. A total of 250 pg of construct and synthetic 5′-capped mRNA (150 pg) encoding a transposase were coinjected into TU-WT embryos at the 1- or 2-cell stage, with 1% of phenol red as a tracer. Microinjection was performed under a dissection microscope (MZ8; Leica) fitted with a MPPI-2 pressure injector (ASI Systems, Omaha, NE, USA). The expression of eGFP was analyzed by direct observation of eGFP fluorescence under a fluorescence stereoscope and a confocal microscope. The number of embryos positive for eGFP fluorescence was determined, and the fluorescence distribution was compared between different Tg lines to score activity and tissue specificity.

Morpholino knockdown

Antisense morpholino oligonucleotides (MOs; GeneTools, Philomath, OR, USA) were designed against *runx2a*, *runx2b*, and *runx3*, as previously described, including a splice-target MO against both *runx2a* isoforms and translational start blocking MOs targeting of each isoform of *runx2b* (*runx2bT1* and *runx2bT2*) and *runx3* (31, 32). A scrambled MO with no known target in zebrafish, cMO, 5′–CCTCTTACCTCAGTTACAATTTATA–3′ was used as control. In addition, *runx*-MOs and/or *p53* (*p53*-MO) (33) were also used to target *runx* and *p53* genes, respectively. The MOs were resuspended in water to a final concentration of 0.5 mM. Approximately 2 nl was injected into 1- or 2-cell stage Tg reporter embryos. Knockdown embryos were analyzed for eGFP fluorescence at 2 dpf, and *pth4* transcription was assessed by ISH and real-time qPCR.

Two-photon laser ablation

Embryos were mounted, imaged, and cells ablated as previously described (34). pth4:eGFP and bactin2:mCherry double-positive Tg zebrafish were visualized throughout development. The hypothalamic area was imaged *in vivo* at 1, 2, 3, and 7 dpf. The 2 clusters of eGFP-expressing cells and the number of cells in each stage of development were evaluated by analyzing each 2 μm-thick *z*-plane slice from a full confocal z-stack projection and scored. Two rounds of ablations were performed per experimental embryo at different time points (1 and 2 dpf). This protocol was chosen as the most efficient of several attempted iterations for a complete ablation process at each time point and to achieve low neuronal recovery during development. Afterward, ablated and control larvae were imaged as full *z*-stack images to monitor recovery of the Pth4-expressing neurons.

Micro-CT scanning and whole-body mineral contents

Volumetric bone mineral density (vBMD) and whole-body calcium, phosphorus, and magnesium were determined in TU-WT and Tg(Xla.Eef1a1:pth4)iim010 adult male zebrafish ($n = 20$). Fish were euthanized with 2-phenoxyethanol (1:500), fixed in 2% PFA, and scanned with a high-resolution micro-CT SkyScan 1172 (micro-CT NV; Bruker, Kontich, Belgium) at 60 KV X-ray source voltage and 167 μA source current with an image pixel size of 5 μm. Internal structures were reconstructed according to the Feldkamp convolution back-projection algorithm (35). In the scanned area, including a portion of the head and the rostral portion of the spine, 4 different volumes of interest (VOIs) were selected to determine the vBMD, using standard software provided with the equipment (SkyScan CT-Analyzer 1.10.0.2; Bruker). vBMDs were calculated by direct calibration against the attenuation coefficients of 2 hydroxyapatite phantoms with known densities (250 and 750 mg/cm^3).

For whole-body calcium, phosphorus, and magnesium determination, fish were freeze dried until dry (dry weight) and dissolved in concentrated nitric acid (70%; 3 ml/g dry weight; Sigma-Aldrich). Nitric acid sample digestion were diluted 500-fold with demineralized water and analyzed for calcium, phosphorus, and magnesium using inductively coupled plasma optical emission spectrophotometry (4300 DV, Optima; Perkin Elmer). Mineral content was expressed in milligrams per gram dry weight, based on the fish dry weight and the total sample digestion volume.

Statistics

Data are expressed as means ± SEM. Differences between groups were assessed by Student's *t* test. A value of $P < 0.05$ indicated statistical significance. Comparisons between numerical data were evaluated by 1-way ANOVA with the Tukey's *post hoc* test. Data were deemed to be statistically similar if they shared at least 1 letter. Statistical analysis and figures were performed with PASW Statistics 18.0 (SPSS; IBM, Armonk, NY, USA) and SigmaPlot 12.0 (San Jose, CA, USA), respectively.

RESULTS

Identification and genomic characterization of the *pth4* gene

Using BLAST analysis, we identified a previously unannotated new zebrafish paralog of the *pth* gene family on zebrafish chromosome Dre22: 597996-600181 (GRCz10) that we call *pth4*. Results from 5′- and 3′-RACE revealed that the *pth4* full-length transcript was 809 bp long and consists of an open reading frame of 366 bp, a 94-bp 5′-UTR and a 349-bp 3′-UTR (Supplemental Fig. S1). Aligning the

cDNA to the genome sequence predicted that the *pth4* gene structure consists of 2 exons and 1 intron. The *pth4* cDNA predicted translation was a 121-aa sequence that contained a secretion signal sequence of 24 aa in the N terminus (*http://cbs.dtu.dk/services/SignalP/*), as expected for PTH peptides. Predicted cleavage sites (*http://www.cbs.dtu.dk/services/ProP/*) should yield preprosequences of 31 AAs and a mature peptide of 90 aa. Protein sequence analysis revealed conserved regions including a dibasic cleavage site (RR) and an MHD motif.

Phylogenetic analysis and evolutionary origin of the *pth4* gene

Phylogenetic analyses inferred by maximum likelihood and rooted with Pth protein sequences from the cephalochordate *B. floridae* (36) showed that zebrafish Pth4 belongs to a well-supported clade that includes Pth4 from other teleosts and from spotted gars, coelacanths, chickens, turtles, and 2 marsupial mammals: opossums and Tasmanian devils (**Fig. 1*A***). However, we could identify no *Pth4* genes in human, mouse, or any eutherian mammalian genomes in Ensembl-v79. To investigate the evolutionary relationships of the *pth4* of zebrafish and other teleosts in the context of the entire PTH-related gene family and to better understand the apparent absence of an ortholog of *PTH4* in humans, mice, and other eutherian mammals, we performed a comparative analysis of conserved synteny. Dot-plot analysis of conserved syntenies for 20 Mb encompassing the genomic neighborhood of the human PTH gene located on chromosome 11 revealed that paralogs of most PTH neighbor genes landed on Hsa12 and -19, where *PTHLH* and *PTH2*, respectively, were also located. This finding was consistent with a recent analysis of a 6-Mb window around *PTH2* in Hsa19 (37). The dot plot also revealed other chromosomes, including Hsa1 and -6, with paralogs of numerous PTH neighbor genes, but in which no PTH-related gene has been identified (Fig. 1*B*). This situation would be expected if these regions formed part of the 4 paralogons that would have been generated by the 2 rounds of WGD that took place during early vertebrate evolution (38, 39) [reviewed in Cañestro (40)]. Analysis of gene clusters using the Synteny Database (16) revealed that paralogs of 21 of the 28 closest neighbor genes to the zebrafish *pth4* gene in Dre22 were located in Hsa1 or -6 (Supplemental Fig. S2). Comparison of the genomic neighborhood of *Pth4* in chromosome 26 of chickens (Fig. 1C; Gga26), which is more closely related to humans than to zebrafish, revealed that paralogs of 9 of the 10 nearest neighbor paralogs in a 150-kb window are

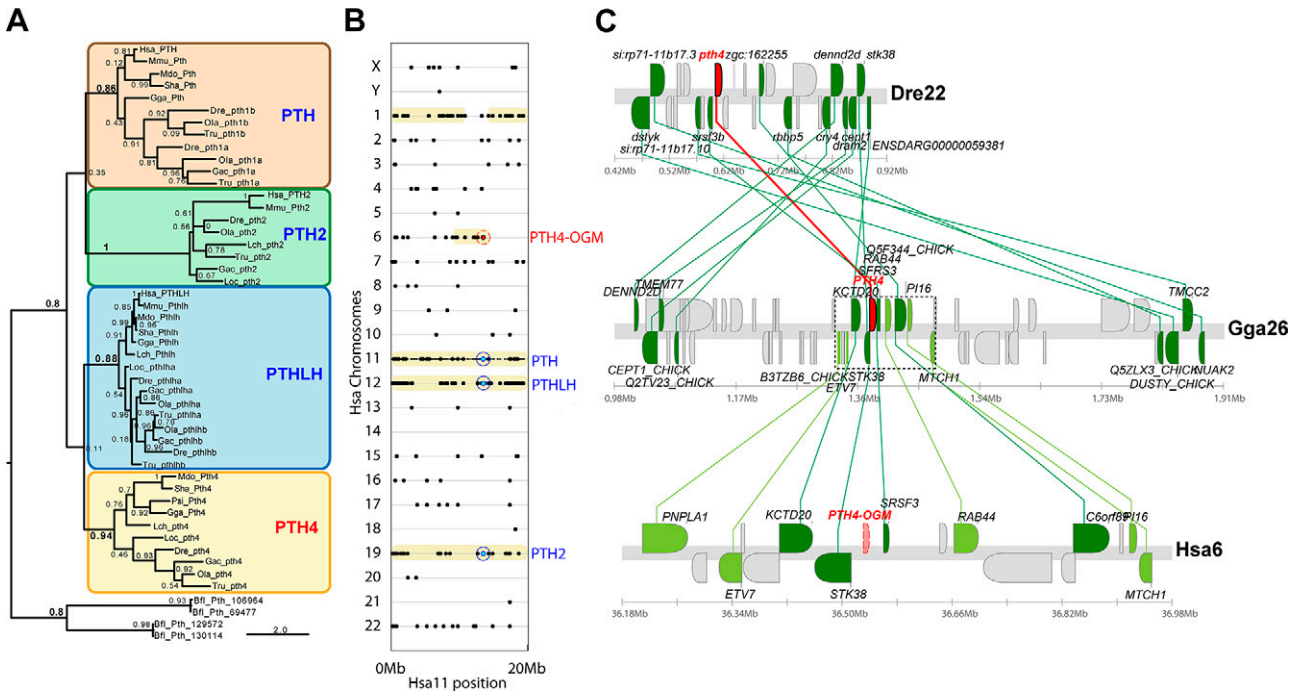

Figure 1. Phylogenetic and conserved synteny analysis of PTH related proteins. *A*) A phylogenetic tree inferred by maximum likelihood, showing the relationship between PTH4 proteins and other proteins of the PTH, PTH2, and PTHLH families. *B*) Dot-plot analysis shows the distribution of paralogs (black dots) of the PTH neighbor genes in the first 20 Mb of human chromosome 11 (Hsa11 on the *x* axis) throughout all chromosomes of the human genome (*y* axis) using both the amphioxus *B. floridae* and the ascidian *C. intestinalis* genomes as outgroups. Yellow shadow areas highlight conserved syntenic regions that probably originated in 2 rounds of WGD that took place during early vertebrate evolution (38, 39) [reviewed in Cañestro (40)], including Hsa12 and -19, where the ohnologs PTH2 and PTHLH are located (blue circles), and other regions including Hsa1 and -6, where PTH ohnologs are missing (PTH-OGM, red circle). *C*) Analysis of the Synteny Database revealed that the genomic neighborhoods of the *pth4* gene in zebrafish and chickens show extensive conserved synteny with Hsa6, suggesting that the putative paralogon region in which the ancestral PTH4-OGM should have been located before it was lost (transparent red) in the lineage leading to humans after the split of the lineage leading to current armadillos, whereas it has been preserved (red) in chicken Gga26 and teleosts such as in zebrafish Dre22. Sequence references may be found in Supplemental Fig. S3.

specifically in Hsa6. This finding strongly suggested that an ancestral PTH4 ohnolog was present in the last common ancestor of ray-finned fish (Actinopterygii, including zebrafish) and lobe-finned fish (Sarcopterygii, including coelacanths, chickens, and humans), but was lost in the lineage leading to humans after the eutherian–metatherian split; furthermore, our analysis revealed that the PTH4-OGM (ohnolog gone missing) should have been in Hsa6 before it was lost, whereas it was preserved in other noneutherian vertebrate lineages, including chickens and teleosts, such as zebrafish.

Temporal and spatial expression of *pth4* during embryonic and larval development

We examined the spatial expression of *pth4* by ISH in zebrafish. Starting at 24 hpf, embryos displayed *pth4* expression in 2 bilateral spots in the lateral ventral diencephalon corresponding to the region of the developing hypothalamus (**Fig. 2*A*, *B***). We observed a gradual number and movement of cells within the 2 bilateral clusters during development (Fig. 2*A*–*F*). At 3 dpf, *pth4* appeared to be specifically expressed by 2 subsets of neurons in the lateral hypothalamus, distant from *pth2*-expressing cells (Fig. 2*G*, *H*). In adult fish (360 dpf), bilateral cell clusters were detected in the dorsal zone of the periventricular hypothalamus (Fig. 2*I*). Expression of endogenous *pth4* was never detected by eGFP expression and ISH outside this hypothalamic area in embryonic and later stages. Analysis of temporal expression of *pth4* by real-time PCR (Fig. 2*J*) revealed that *pth4* was maternally transcribed, being detected in embryos as early as 0 hpf and showing a progressive decrease until 9 hpf. Zygotic expression of *pth4* appeared to increase from 12 hpf through subsequent development and then to increase at 4, 5, and 6 dpf.

A neural network for *pth4*-expressing cells

Having shown that *pth4* was specifically expressed in the hypothalamus, we generated independent zebrafish Tg lines containing eGFP reporter constructs including 1 kb (P1 = *1kb-pth4-Tol2-eGFP*) or 2 kb (P2 = *2kb-pth4-Tol2-eGFP*) fragments upstream of the *pth4* TSS. A search for eGFP signal in all P1 and P2 Tg zebrafish lines and in situs to the pth4 transcript was performed carefully throughout the organism and showed that the eGFP expression patterns replicated the spatiotemporal pattern of endogenous pth4 transcript (**Fig. 3**). At 1 dpf, the P2 line labeled 2 bilateral clusters of 4–6 neural bodies, each as well as their axonal projections, which extended both to the anterior and posterior part of the brain from the lateral hypothalamus (Fig. 3*A*, *B*). Double labeling experiments showed a robust colocalization of endogenous *pth4* transcripts and eGFP signal (Fig. 3*C*–*C*″). At 3 dpf, the number of labeled neuronal bodies had increased up to 14 per cluster, and long neural projections labeled by eGFP extended ventrally from the caudal part of the diencephalon through the midbrain and hindbrain and along the spinal cord (Fig. 3*D*, *E*). Posterior projections were arranged in 2 parallel axes showing long-range neuronal fibers running through

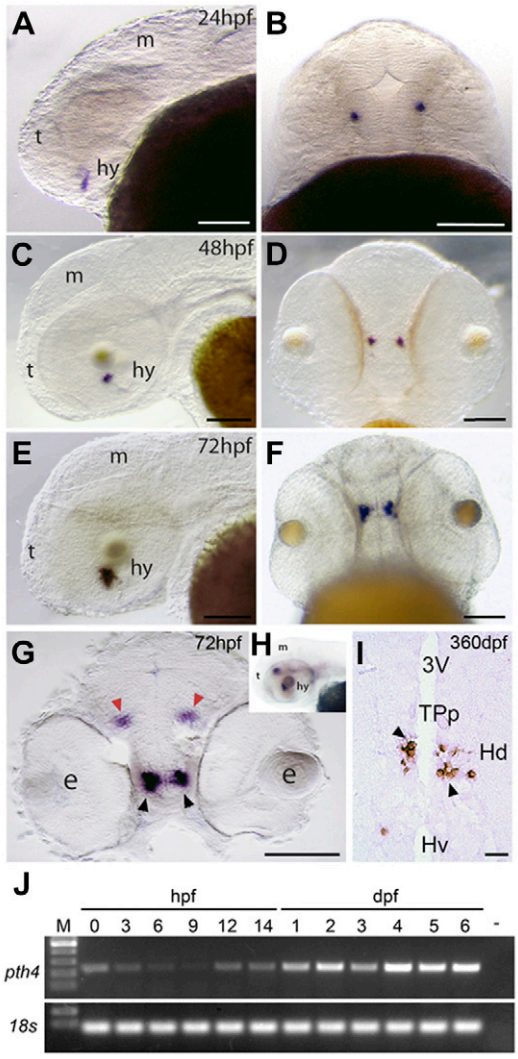

Figure 2. Spatial and temporal expression of PTH 4 (*pth4*) transcripts in zebrafish embryos. *A*–*F*) Gradual movement of the expression domain during development from caudoventral to a more rostrodorsal situation with reference to the eye position. Lateral (*A*, *C*, *E*) and ventral (*B*, *D*, *F*) views of whole-mount ISH of *pth4* expression of 1 dpf (*A*, *B*), 2 dpf (*C*, *D*), and 3 dpf (*E*, *F*) wild-type zebrafish embryos. Staining with the *pth4* antisense probe showed expression in bilaterally symmetric regions of the developing hypothalamus. *G*, *H*) Rostrocaudal transverse sections (4 μm thick) of Epon-embedded, whole-mount double ISHs of *pth2* (*G*, red arrowheads) and *pth4* (*G*, black arrowheads) in 3 dpf zebrafish identified *pth4* expression domains in the lateral hypothalamus (*H*). *I*) Rostrocaudal transverse section (10 μm thick) of paraffin-embedded ISH of *pth4* expression in adult zebrafish displayed *pth4* transcripts exclusively in bilateral cell clusters located in the dorsal zone of the periventricular hypothalamus. *J*) Real-time PCR analyses of the temporal expression pattern of *pth4* mRNA. e, eye; Hd, dorsal zone of the periventricular hypothalamus; hy, hypothalamus; Hv, ventral zone of the periventricular hypothalamus; m, midbrain; t, telencephalon; TPp, periventricular nucleus of posterior tuberculum; 3v, third ventricle. Scale bars: 100 μm (*A*–*G*); 5 μm (*I*).

the spinal cord (Fig. 3*F*). At 5 dpf, the number of neural cell bodies did not appear to have changed, but projections formed a complex and branched neural network (Fig. 3*G*). One-year-old adult fish showed a high density of branched fibers around the cluster of neurons in the dorsal

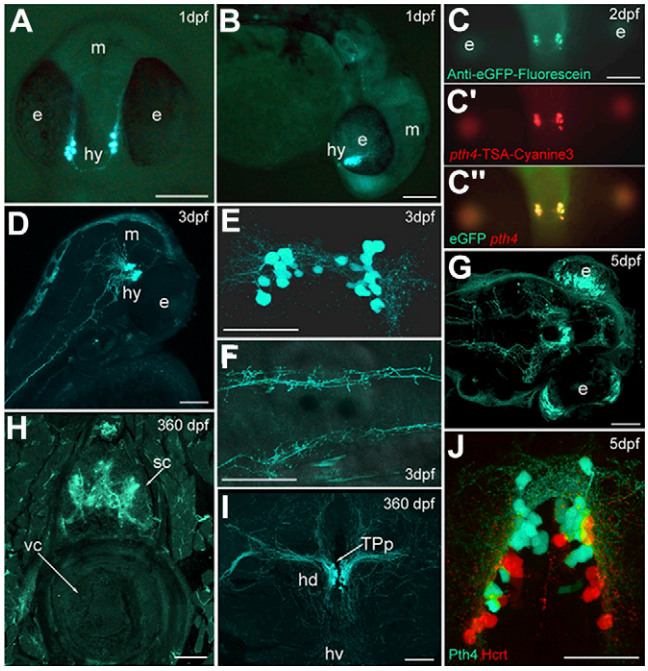

Figure 3. Whole-mount confocal imaging of the stable Tg(pth4: eGFP)iim07 zebrafish line. *A–G*) Pth4 cells and projections at 1 (*A*, *B*), 2 (*C–C″*), 3 (*D–F*), and 5 dpf (*G*) monitored as eGFP fluorescence. Double labeling of eGFP immunofluorescence and fluorescence *pth*4 ISH (FISH) on 3-dpf Tg(pth4: eGFP) iim07 zebrafish line (*C–C″*) demonstrates identical expression of eGFP (green color) and endogenous *pth*4 transcripts (red). Confocal imaging of 25-μm cross-sections from adult fish, showing the Pth4 anterior–posterior caudal projections in the spinal cord (*H*) and Pth4 bilateral clusters in the periventricular hypothalamic area (*I*). *J*) Double pth4:eGFP and hcrt:tdTomato zebrafish line showing the specific spatial colocalization of Pth4 and Hcrt neural clusters in the lateral hypothalamus at 5 dpf. e, eye; hd, dorsal hypothalamus; hv, ventral zone of periventricular hypothalamus; hy, hypothalamus; m, midbrain; SC, spinal cord; TPp, periventricular nucleus of posterior tuberculum; VC, vertebra centra. Scale bars: 100 μm (*A–C*, *F–I*); 50 μm (*J*, *D*, *E*).

area of the periventricular hypothalamus (Fig. 3*I*) and throughout the spinal cord (Fig. 3*H*).

To further characterize the cluster of neural bodies expressing *pth4* in the hypothalamus, we crossed the P2 line to a hcrt:tdTomato line [hypocretin gene (*hrct*), a marker of the lateral hypothalamus in zebrafish embryos] (Fig. 3*J*). Although both genes were expressed in the hypothalamic region, they were expressed in different neural cell types, revealing the presence of different neural subpopulations in this part of the hypothalamus.

The discovery of this complex *pth4*-expressing neural network sending widespread projections from the hypothalamus throughout the brain and spinal cord suggests that Pth4 is a neuropeptide playing a systemic role throughout the entire animal.

Functional characterization of *pth4* promoter and upstream *runx* regulation

The minimal regulatory region required for *pth4* promoter activity was identified by generating serial deletions of the 2-kb promoter sequence upstream of the *pth4* TSS and directed mutagenesis of the 1-kb promoter sequence upstream of the TSS (**Fig. 4*A***). Injection of the *2kb-pth4-Tol2-eGFP* (n = 174) or *1kb-pth4-Tol2-eGFP* (n = 208) reporter constructs showed the same efficient eGFP expression, suggesting that essential regulatory elements of *pth4* were located in the first 1-kb sequence. Promoter efficiency in all reporter constructs injected was normalized to the *2kb-pth4-Tol2-eGFP* construct activity. Deletion of the region 941–554 bp did not alter the *pth4* pattern replicated by eGFP expression, but decreased the efficiency of expression to 43%. Deletion of the region 544–262 bp, however, resulted in a complete loss of eGFP expression in all of 144 injected embryos, demonstrating that this critical 292-bp fragment contained regulatory elements essential for *pth4* expression. TRANSFAC sequence analysis revealed the presence of at least 6 potential transcription factor-binding boxes within this critical 292 bp (Fig. 4*A* and Supplemental Fig. S4). Mutations designed to disrupt consensus-binding sequences of the predicted transcription factors (Supplemental Fig. S4, red) significantly affected eGFP expression in all injected embryos. Mutations in boxes 1 and 4 decreased the number of embryos expressing eGFP by >50%, similar to the 941–554 deletion (Fig. 4*A*). Mutations in boxes 2, 3, and 5 decreased the efficiency of expression by 77% or more of the injected embryos. Mutation in box 6 resulted in a complete loss of eGFP expression in all injected embryos. This mutated conserved region had homology to the core binding site for RUNX transcription factors. Thus, these results suggested that RUNX transcription factors most likely act as key regulators of *pth4* promoter activity.

The expression pattern of zebrafish *runx* paralogs (*i.e.*, *runx1*, *runx2a*, *runx2b*, and *runx3*) is highly dynamic, and all of them have been described as playing a role in cartilage and bone development (31). Among these paralogs, the *runx2a* expression pattern includes a bilateral domain compatible with the 2 clusters of *pth4*-positive cells in the hypothalamus (41, 42). To test whether zebrafish Runx2a regulates the *pth4* promoter *in vivo*, we used *runx2a*-specific antisense morpholino-knockdown approach and tested for *2kb-pth4-Tol2-eGFP* activity, as well as for *pth4* expression. Knockdown by injecting *runx2a*-MO into the P2 reporter line revealed that by 2 dpf, the formation of the 2 clusters of neuronal eGFP-positive cell bodies was significantly altered: 6.3% of injected embryos did not show any *pth4* positive cells, 41.4% showed absence of one of the neural clusters and the other was severely reduced (in most cases only 1 cell), and 52.3% showed 2 clusters but with a reduced number of positive cells (Fig. 4*B*, *C*). To provide further evidence that the *runx2a* morphant phenotypes are specific and not related to nonspecific off-target effects [*e.g.*, p53 mediated apoptosis (33)], we also analyzed eGFP expression *in vivo* in *runx2a* morphants that were coinjected with a *p53* morpholino. Similar to previous experiments, the formation of the 2 $eGFP^+$ clusters of neurons was severely affected suggesting that our phenotype was not caused by nonspecific apoptosis (Fig. 4*D*). Animals injected with *p53*-MO alone did not exhibit a phenotype in our region of interest (data not shown). Moreover, WISH (Fig. 4*E–G*) as well as real-time qPCR (Fig. 4*H*) showed significant reduction of *pth4* transcript

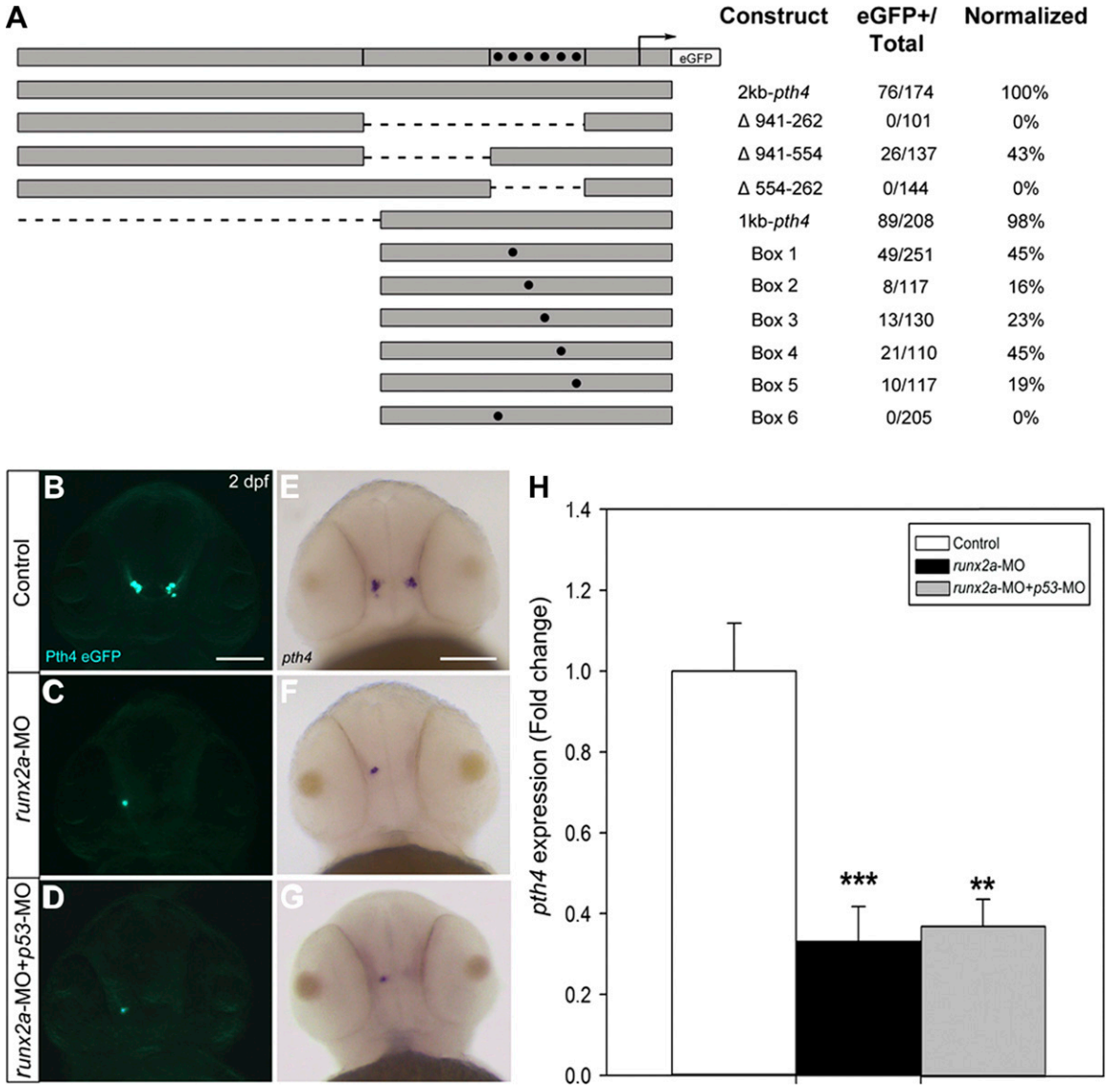

Figure 4. Functional analysis of the pth4 promoter through eGFP expression. *A*) DNA fragments containing 2- and 1-kb sequences upstream from the ATG of *pth4* are in gray. Vertical lines mark increments of the functional 2kb-*pth4* promoter deleted. Filled circles: conserved regions selected for mutations. Box 1, positions 507–513 (TFBSs): CREB/HRE/ATF6); box 2, 433–439 (TFBS: HMX2/LXRE); box 3, 397–402 (TFBS: HOXA5/BRN5/LHX6/VAX2/ISL1); box 4, 329–338 (TFBS: AP1/NFE2/MEIS1/PBX1_MEIS1/VDR_RXR); Box 5, 321–323 (TFBS: VMAF/CREB/MARE); and box 6, 518–522(TFBS: RUNX2/RUNX3). Arrow and hatched section: the start of transcription and 5′UTR, with eGFP coding sequences substituting at the native TSS. Promoter activity was assessed as the proportion of embryos displaying 1 or more fluorescent Pth4 cells at 3 dpf and normalized to the wild-type 2kb-*pth4* promoter results. *B–H*) Knockdown of *runx2a* affects *pth4* expression. *B–D*) Morphology of the control (*B*, ventral view), *runx2a*-MO-injected (*C*, ventral view), and *runx2a*-MO- and *p53*-MO-injected (*D*, ventral view) Tg(pth4:eGFP)iim07 embryos at 48 hpf. Note the reduced eGFP fluorescence in the *runx2a*-MO-injected embryos. Scale bars, 100 μm. *E–G*) WISH using *pth4* riboprobe on control (*E*, ventral view), *runx2a*-MO-injected (*F*, ventral view), and *runx2a*-MO- and *p53*-MO-injected (*G*, ventral view) Tg(pth4:eGFP)iim07 embryos at 48 hpf. Note the reduced *pth4* expression in the *runx2a*-MO-injected embryos. *H*) Real-time qPCR analysis of *pth4* expression in control (white bars), *runx2a*-MO-injected (black bars), and *runx2a*-MO- and *p53*-MO-injected (gray bars) Tg(pth4:eGFP)iim07 embryos at 48 hpf. Results normalized to *eef1a1/1* expressed as means ± SEM of 2 independent experiments. $^{**}P < 0.025$, $^{***}P < 0.01$.

expression in *runx2a* morphants, similar to the decrease of expression observed for eGFP.

Results from the promoter deletions and direct mutagenesis, together with knockdown experiments, show that Runx2a is a direct upstream activator of *pth4* expression. That the expression of *pth4* was not completely abolished in 100% of the animals and that MOs against *runx2bT1*, *runx2bT2*, and *runx3* also affect *pth4* expression (unpublished results), suggest the possibility of a certain degree of redundancy or cooperative action among *runx* paralogs.

Pth4 interacts with all 3 zebrafish Pth receptors

Analysis of the zebrafish genome revealed the presence of 3 Pth receptors (*i.e.*, Pth1ra ENSDARG00000020957, Pth1rb

ENSDARG00000018418, and Pth2r ENSDARG00000006678) that can act downstream of Pth4. To determine whether a specific receptor mediates Pth4 signaling, we expressed zebrafish Pth receptors in HEK cells and performed a cAMP-based β-galactosidase reporter gene assay. All receptors showed similar basal induced cAMP production. Pth4 stimulation induced a dose–response increase in cAMP production and no significant differences were detected with any of the 3 receptors transiently transfected (**Fig. 5*A*, *B***). These results suggest that Pth4 signaling could be mediated promiscuously by all 3 Pth receptors. We also transfected cells with human Pth and found that all 3 zebrafish receptors increased cAMP production, with Pth1ra being activated the most efficiently and Pth2r the lowest, which is consistent with *in vitro* analysis published using human PTH and zebrafish receptors (25) (Fig. 5*B*). It is interesting to note that zebrafish Pth4 activated Pth1ra with efficiency similar to that of human PTH, suggesting that human PTH (*i.e.*, PTH1) and zebrafish Pth4 exert equivalent effects at the ligand–receptor level.

In humans, PTH peptides play crucial roles in bone homeostasis *via* PTH1R on osteoblasts (43). Therefore, in addition to Pth4-Pthr signaling, we also analyzed the spatial expression of zebrafish *pth1ra* in adult zebrafish. Expression of *pth1ra* was specifically found in gills (Fig. 5*C*, *D*); craniofacial bones, such as ceratobranchial and operculum (Fig. 5*C*); intestinal epithelium (Fig. 5*E*), and spinal cord (Fig. 5*F*). These results are consistent with a Pth4-Pth1ra signaling pathway controlling bone mineral metabolism through the main target organs (*i.e.*, gills, intestinal epithelium, and bone) that are known to promote ionic fluxes *via* absorption/reabsorption or mobilization.

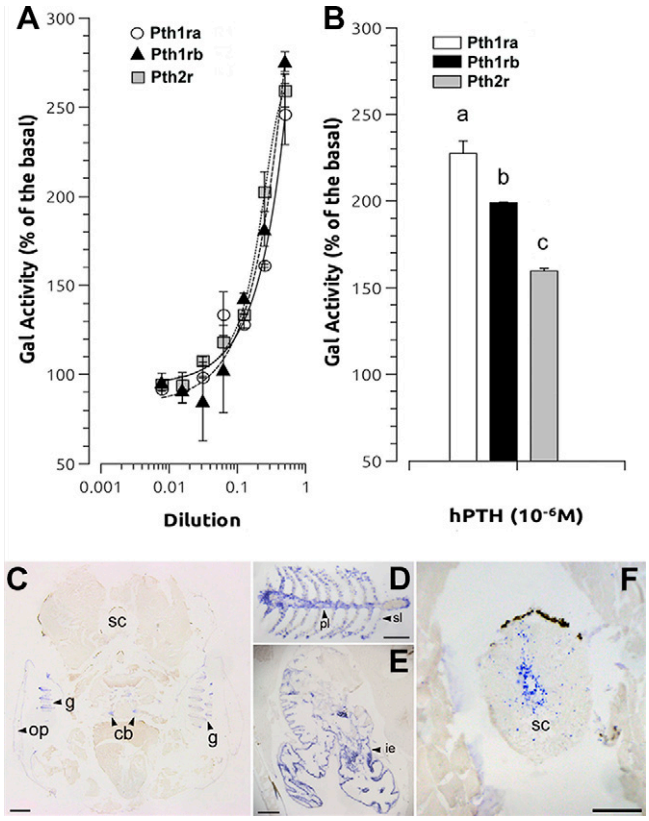

Figure 5. Pth4 interaction with zebrafish Pth receptors. *A*, *B*) Effects of recombinant Pth4 mature peptide dilutions (*A*) and synthetic hPTH (*B*) on galactosidase activity in HEK293 cells stably expressing cAMP-responsive β-galactosidase reporter gene and transiently transfected with zebrafish *pth1ra*, *pth1rb*, and *pth2r* genes in the presence of a phosphodiesterase inhibitor, IBMX. Results represent the means ± SEM of 2 independent biological replicate experiments, each performed with 3 technical replicates. Measurements were normalized for protein content and expressed as a percentage of basal levels (HEK293 cells transfected with empty pcDNA3 vector). Values of $P < 0.05$ (indicated by letters on bars) were considered statistically significant. Data are statistically similar if bars share at least 1 letter. *C–F*) ISH of adult zebrafish sections shows specific *pth1ra* expression in gills (*C*, *D*), craniofacial bones (*C*), intestine (*E*), and spinal cord (*F*). g, gills; op, opercular bone; cb, ceratobranchial bone; sc, spinal cord; pl, primary lamella; sl, secondary lamella; ie, intestinal epithelium. Scale bars: 400 μm (*C*); 50 μm (*D*); 200 μm (*E*); 100 μm (*F*).

Targeted *pth4*-expressing neuron ablation results in reduced bone mineralization during embryo development

Using the zebrafish Tg(pth4:eGFP)iim07 Tg line, in which Pth4-expressing neurons were labeled by eGFP (Fig. 3), 2-photon laser ablation was used to eliminate the mCherry-positive nuclei (bactin2:H2A-mCherry) of individual pth4:eGFP-positive neural bodies in the hypothalamus at 2 sequential time points (1 and 2 dpf). Successful ablation was demonstrated by the instant loss of mCherry and subsequent loss of eGFP (**Fig. 6*A–D***). Observations of the morphology after ablation did not uncover damaging effects to neighboring tissue. When examining ablated larvae at 7 dpf, 5 d after conducting the double (1 and 2 dpf) laser ablation protocol, the lack of pth4:eGFP-positive neural bodies was evident in comparison to control larvae (Fig. 6*B*, *D*). Absence of pth4:eGFP-positive neurons resulted in a significant decrease in Pth4 expression levels, as assayed by whole-embryo real-time qPCR (Fig. 6*I*). A 2-color acid-free cartilage and bone stain (Fig. 6*E–H*) showed that ablated larvae showed a marked decrease in bone mineralization of craniofacial structures, such as the notochord tip, operculum, otolith, cleithrum, and ceratobranchial arch 5 at 7 dpf, whereas the formation of head cartilage was unaffected. These experiments, therefore, suggest that the pth4:eGFP-positive neurons in the hypothalamus are essential brain regulators of bone mineralization. Likewise, it is important to remark that ablating pth4-expressing neurons should affect all factors downstream of Pth4, so the effect we detect in bone mineralization could be secondary to the release of other factors from the brain that act downstream of Pth4.

Overexpression of *pth4* induces loss of BMD and changes in whole-body mineral contents in Tg zebrafish

To investigate the biological role of Pth4 in adult fish, we created a zebrafish Tg line ubiquitously expressing *pth4* driven by the *eef1a1* promoter Tg(Xla.Eef1a1:pth4)iim010. The strong, widespread, and stable Tg Pth4 expression was assessed by real-time qPCR (Supplemental Fig. S5).

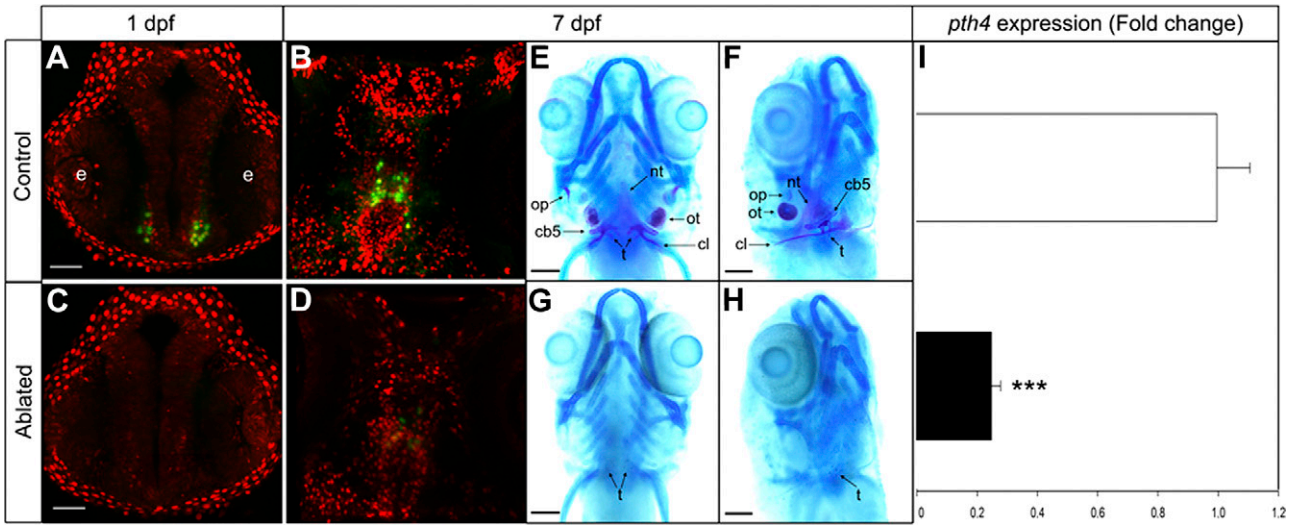

Figure 6. Two-photon laser ablation of Pth4 neurons. *A–D*) Whole-mount confocal imaging of the pth4:eGFP$^+$/bactin2:H2A-mCherry$^+$ double Tg embryo, showing the Pth4 neural hypothalamic bodies at 1 (*A*, *C*) and 7 dpf (*B*, *D*), monitored as eGFP fluorescence in control (*A*, *B*) and laser-ablated (*C*, *D*) embryos. *E–H*) Two-color acid-free cartilage and bone staining of control (*E*, ventral view, and *F*, lateral view) and Pth4 neuron-ablated (*G*, ventral view, and *H*, lateral view) 7 dpf embryos. Note the lack of mineralized craniofacial bones with an incipient mineral deposit on teeth in Pth4 neuron ablated embryos. *I*) Real-time qPCR analysis of *pth4* expression in control (white bars) and Pth4 neuron-ablated (black bars) embryos at 7 dpf. Results are normalized to *actb1* and expressed as means ± SEM of 2 independent experiments. nt, notochord tip; op, operculum; ot, otolith; ceratobranchial arch 5 (cb5); t, teeth; cl, cleithrum; e, eye. Scale bars: 50 μm (*A–D*) 100 μm (*E–H*). ***$P < 0.01$.

Characterization of whole-body mineral contents (*i.e.*, calcium, phosphorus, and magnesium) by spectrophotometry in adult male zebrafish ($n = 20$) showed a significant decrease in minerals in *pth4* Tg fish compared with control TU-WT (**Fig. 7*A***). We wondered whether the decrease in whole-body mineral contents could be related to ion mobilization from bone. To test this hypothesis, we analyzed volumetric bone mineral density (vBMD) and found a significantly lower vBMD in all volumes of interest analyzed in *pth4* Tg zebrafish ($P < 0.01$; Fig. 7*B*). We concluded, therefore, that Pth4 can mobilize minerals from bone to extracellular fluids and then the increase of mineral concentration at the extracellular level leads to its removal from the body, which affects calcium/phosphorus composition in the whole-body and skeletal structure.

Phosphate homeostasis is disrupted in *pth4* Tg zebrafish

To investigate whether *pth4*-dependent changes in body calcium/phosphorus contents and in vBMD could be related to alterations in expression levels of genes involved in mineral homeostasis, we performed real-time qPCR to determine the levels of expression of several phosphocalcic metabolism regulatory genes (Supplemental Table S1) in adult fish of both TU-WT and *pth4*-Tg lines (**Fig. 8**). Results revealed that *pth4*-Tg fish had a significant ($P < 0.05$) up-regulation of the solute carrier family 34 type II sodium/phosphate cotransporter member 2b gene (*slc34a2b*, *npt2b*) but a significant ($P < 0.01$) down-regulation of a set of phosphate-regulating genes, including the endopeptidase on the X chromosome (*phex*), ectonucleoside triphosphate diphosphohydrolase 5 (*entpd5*), and solute carrier family 34 type II sodium/phosphate cotransporter member 1a (*slc34a1a*, *npt2a*). Notably, the down-regulation of *npt2a* was accompanied by a significant ($P < 0.025$) up-regulation of *fgf23*, which has been described as a key regulator of phosphate homeostasis (44). Finally, no significant differences were found on stanniocalcin-1-like (*stc1l*) gene expression levels. Overall, results of *pth4*-overexpression experiments revealed that *pth4* not only had an important role affecting the expression of effector proteins responsible for bone metabolism through regulation of phosphate homeostasis (*i.e.*, *npt2a*, *npt2b*, *phex*, and *entpd5*) but also affected a regulatory pathway (*fgf23*).

DISCUSSION

The ancestral Pth4, which was lost in eutherian vertebrates, is a regulator of bone homeostasis

The PTH gene family regulates bone homeostasis in vertebrates. To date, 3 ohnologs have been described—PTH, PTH2, and PTHLH (45)—that appear to have originated *via* 2 rounds of 1R/2R WGDs during early vertebrate evolution (38) (**Fig. 9*A***). In teleosts, moreover, *pth* and *pthlh* each have 2 paralogs—*ptha/pthb* and *pthlha/pthlhb*—that originated in the extra round of WGD that occurred during early teleost evolution (3R or teleost genome duplication) (37). We identified and characterized a novel Pth family member, Pth4. Our phylogenetic inferences and analysis of conserved syntenies shared by the *pth4* genomic neighborhood in zebrafish and its ohnologons in chickens and humans provide evidence consistent with the hypothesis that Pth4 is the fourth missing PTH ohnolog resulting from 1R/2R-WGDs. Our genome survey shows that Pth4 is present in ray-finned fish and in noneutherian

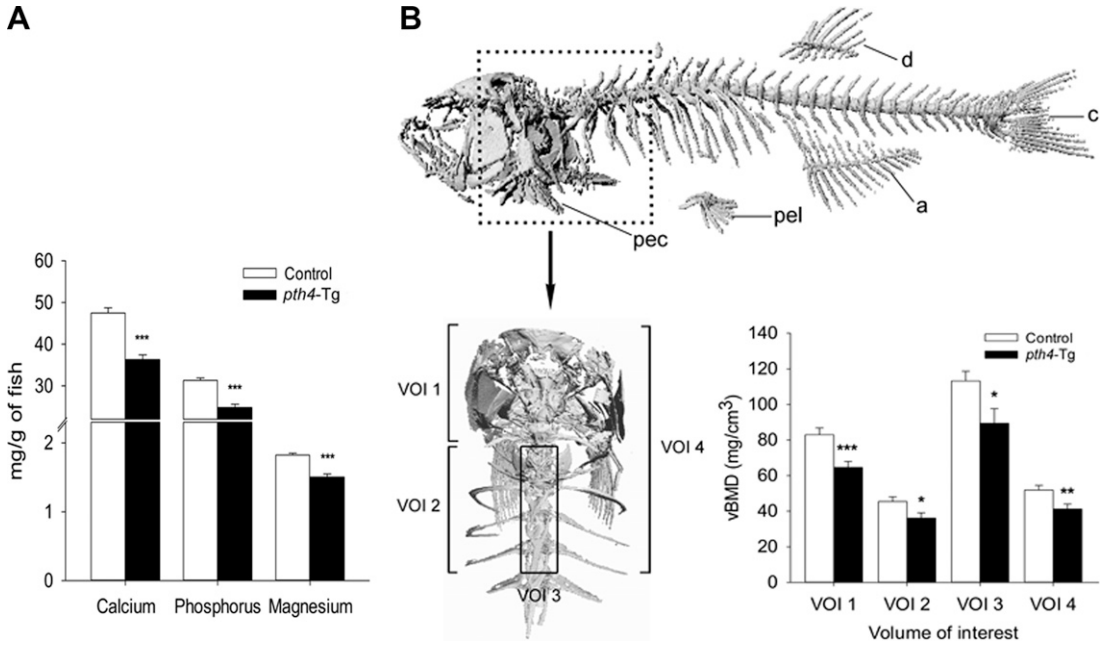

Figure 7. *A*) Whole-body calcium, phosphorus and magnesium analysis. *B*) Representative images for VOI1: end lapilli otoliths to end of sagittal otoliths; VOI2: end sagittal otoliths to 5 vertebrae (included pectoral fins and scales); VOI3: end sagittal otoliths to 5 vertebrae but includes only a cylinder (diameter of 1 mm) with the center in the middle of the vertebral bodies; and VOI4: VOI1+VOI2; and vBDM analysis. a, anal fin; c, caudal fin; d, dorsal fin; pec, pectoral fin; pel, pelvic fin. Results are expressed as means ± SEM. $*P < 0.05$, $**P < 0.025$, $***P < 0.01$.

vertebrates but absent in eutherians because of a gene loss that likely occurred at the base of the eutherian mammalian clade (*i.e.*, a eutherian OGM; Fig. 9*A*). For the sake of clarity and to better reflect the evolutionary origin of the Pth family, we propose a change in the nomenclature of this vertebrate family, in which PTH and PTHLH should be renamed to PTH1 and -3, respectively. Accordingly, after the nomenclature of teleost genes duplicated during the 3R, *ptha* and *pthb* should be thought of as *pth1a* and *pth1b; pth2* remains as *pth2; pthlha* and *pthlhb* should be thought of as *pth3a*; and *pth3b* and the newly identified gene should be called *pth4*.

From brain to bone: Pth4, a hypothalamic neural signaler downstream of Runx that regulates bone remodeling in zebrafish

Expression analysis during zebrafish development revealed that *pth4* is maternally transcribed. By 24 hpf, however, *pth4* is expressed exclusively in a bilateral subset of neurons located in the hypothalamus. Transgenic reporter lines expressing eGFP under the *pth4* and *hrct* promoters identified 2 distinct subpopulations of neuronal cell bodies in the lateral hypothalamus. The pth4:eGFP reporter line also mapped a *pth4*-positive complex network of long axonal projections from the dorsal zone of the periventricular hypothalamus to the brainstem and spinal cord. Promoter dissection identified a region of 544–262 bp that is critical for *pth4* expression. Results of TRANSFAC sequence prediction, promoter region deletions and directed mutagenesis uncovered 5 potential regulatory elements driving *pth4* expression. In particular, Runx-factor binding sites appeared to be critical for *pth4* expression. Loss of Runx2a activity abrogated both *pth4* expression and the activity of the pth4:eGFP reporter line, demonstrating that *pth4* is downstream of *runx2a*. In mammals, RUNX2 is a multifunctional transcription factor implicated in bone development and mineralization by

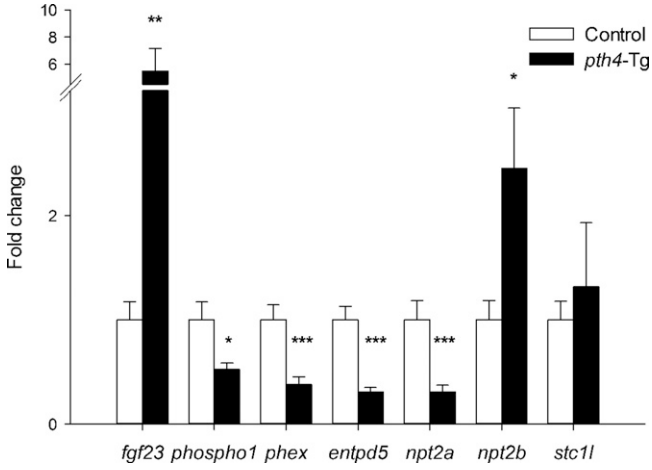

Figure 8. Phosphate homeostasis is disrupted in *pth4* Tg fish. Real-time qPCR analysis of mineral homeostasis regulatory factors in TU-WT (white bars) and Tg(Xla.Eef1a1:pth4)iim010 adult male zebrafish (black bars). mRNA expression levels of fibroblast growth factor 23 (*fgf23*), phosphatase orphan 1 (*phospho1*), phosphate-regulating gene with homologies to endopeptidase on the X chromosome (*phex*), (*entpd5*), solute carrier family 34 (type II sodium/phosphate cotransporter), member 1a (*slc34a1a*, *npt2a*), member 2a (*slc34a2a*, *npt2b*), and stanniocalcin-1-like (*stc1l*) were determined. Results normalized to *18S* are expressed as means ± SEM of 2 independent experiments. $*P < 0.05$, $**P < 0.025$, $***P < 0.01$.

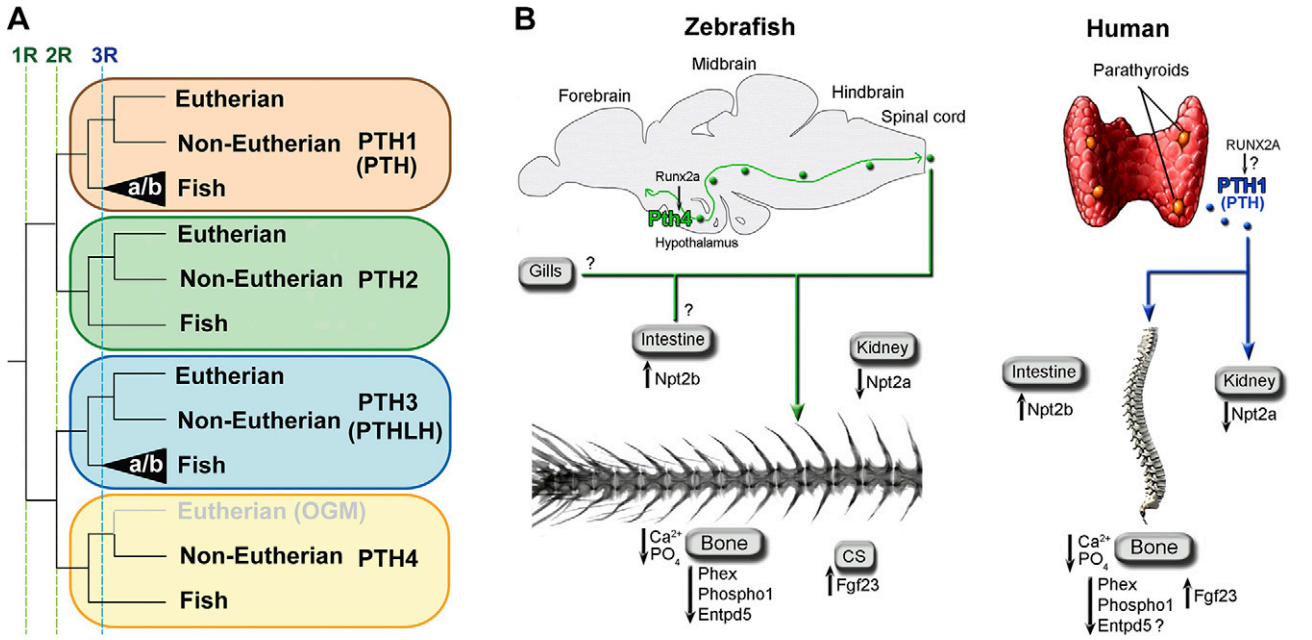

Figure 9. Evolutionary history of the PTH family in vertebrates. *A*) Analysis reveals 4 PTH ohnologs (PTH1–4) that arose because of 2 rounds of 1R/2R WGD in early vertebrates and third round (3R) in teleosts (a/b paralogs). The absence of Pth4 in eutherian mammals is related to an ancestral gene loss that likely occurred when this clade diverged from metatherian mammals. *B*) This loss is concomitant with the recruitment of PTH1 from parathyroid glands in eutherians to provide an equivalent function to the Pth4 neuropeptide in bone mineral homeostasis, as it is represented by zebrafish and human diagrams, in which both PTH peptides provoke similar responses in phosphate and calcium homeostasis, acting in bone and regulating the expression of the same regulatory genes in homologous organs.

regulating numerous genes of chondrogenic/osteogenic signaling pathways (46). RUNX2 binding sites have been identified on the *COL10A1* and *SP7* promoter controlling their transcriptional regulation (47, 48). Using the *pth4 eGFP* reporter lines, we demonstrated that the ablation of *pth4*-positive neurons altered bone mineralization during larvae development, affecting craniofacial structures, such as the notochord tip, operculum, otolith, cleithrum, and ceratobranchial arch. However, no difference in cartilage development was found. Taken together, these findings suggest that a population of hypothalamic neurons that express *pth4* under the regulation of the conserved Runx2a bone transcription factor form a complex neural network throughout the body that plays a major role in the mechanisms regulating embryonic bone mineralization in zebrafish.

Pth4 can activate cAMP/PKA signaling *via* Pth receptors and regulates expression of genes involved in calcium/phosphorus homeostasis

Zebrafish *pth4* is predicted to encode a putative protein of 121 aa that includes PTH-specific motifs and dibasic cleavage sites for preprosequences conserved in other secreted members of the PTH family (11, 49). We demonstrated that Pth4 can recognize the 3 zebrafish Pth receptors (*i.e.*, Pth1ra, Pth1rb, and Pth2r) to activate cAMP/PKA signaling. In fish, previous analyses by real-time PCR found that *pth2r* was expressed in the central nervous system, kidney and scales (23, 45, 50), and *pth1rb* in the kidney, intestine, and vertebral bone (51–53). In the current study, WISH revealed that *pth1ra* is expressed in the gills, intestinal epithelium, craniofacial bones, and spinal cord (Fig. 5). The fact that Pth4 shows the same affinity for all 3 receptors in cell culture suggests that this neuropeptide not only acts on the skeleton, either directly or indirectly through the spinal cord, but also, in ectopic/overexpression experiments, has the potential to function in gills, intestine, kidney, and scales, all of which are involved in mineral homeostasis.

Gain-of-function experiments using a Tg line that overexpresses *pth4* demonstrate that an excess of this neuropeptide induces a significant reduction of whole-body calcium/phosphorus levels and results in a significant loss of vBMD, acting through the regulation of phosphate homeostasis. Our analysis of factors involved in the regulation of phosphate levels revealed that *pth4* overexpression induced a significant increase in *fgf23* and *npt2b* levels and a decrease in *npt2a*, *phospho1*, *phex*, and *entpd5* expression levels. FGF23 is a key phosphaturic factor that acts in the bone–kidney axis in mammals and provides a signal from bone to adjust phosphate fluxes through NPT2a in kidney by promoting phosphate excretion or reabsorption (44, 54). In addition, systemic phosphate levels are managed by NPT2b through active transport in the small intestine (55). In zebrafish, *fgf23* is expressed in the corpuscles of Stannius (CS), on the teleost kidney, to regulate ion homeostasis. Expression of *npt2b* in the intestine plays an important role in phosphate absorption (56). Thus, the significant decrease in whole-body phosphorus content in Tg fish could be related to up-regulation of *fgf23* and down-regulation of *npt2a*, which in

turn would produce phosphate excretion through the kidney. Such an effect may be counteracted by phosphate absorption *via* the intestine, consistent with high levels of *npt2b*. In accordance with our results, other studies have demonstrated that loss of function of *phospho1*, *phex*, or *entpd5* in hypophosphatemic disorders led to a significant decrease in vBMD and abnormalities in mineralization (1, 57, 58). One of our most striking results was that despite hypocalcemic conditions in Tg fish, the expression of *stc1l* did not appear to occur, as would be expected from its function in zebrafish (59). This result suggests that anti-hypercalcemic hormones other than *stc1l* (*e.g.*, calcitonin) may act in teleosts to reduce calcium transport across epithelia as its mammalian counterpart (60).

Evolutionary model for the role of the PTH family in bone homeostasis in aquatic and terrestrial vertebrates

Despite the lack of parathyroid glands, fish can respond to changes in serum mineral levels and consequently regulate mineral concentrations within a narrow range. During the past 2 decades, several studies focused on identifying PTH paralogs and explored their involvement in bone mineral balance in vertebrates. Six peptides and 3 receptors had been identified previously, revealing a higher complexity of this gene family in noneutherian vertebrates than in eutherians. Pthlh (*i.e.*, Pth3) has been reported to promote calcium uptake from surrounding water *via* branchial and intestinal epithelia (61), stimulating calcium reabsorption and phosphate secretion through Npt2a in the kidney (53) and promoting osteoclast activity in scales *via* Pthr (62). In addition to calcium uptake, Pth3 seems to affect P_i concentration in the serum of fish species (10). In contrast to placental mammals, no previous evidence supported the hypothesis that Pth1 or Pth2 played a decisive role in mineral balance in fish. In eutherians, PTH1 is considered to be the principal regulator of calcium/phosphate metabolism and bone turnover. This hormone is produced by the parathyroid glands in response to low calcium or high phosphate serum levels and exerts its endocrine function on kidney and bone by interacting with other systemic and local factors, such as vitamin D, FGF23 and calcitonin to restore normocalcemia in a negative feedback loop (63, 64). Our studies suggest that zebrafish Pth4 acts on bone to mobilize calcium and phosphate through Pth1r signaling. Moreover, a PTH-like peptide previously identified in pufferfish and designated PTH-L (here renamed as Pth4) shares a high similarity in the 1- to 34-aa sequence with zebrafish Pth4 and showed calciotropic activity in an *in vitro* scale assay (12). This finding probably reflects the ancestral bony vertebrate condition that has been conserved in noneutherians but lost in eutherian mammals. Concomitantly Pth was recruited to perform an equivalent function in the latter (Fig. 9).

In terrestrial vertebrates, bone provides an internal storage of minerals that have an important metabolic function by mobilizing calcium and phosphate for mineral homeostasis. In fish, calcium-driven mineral homeostasis has been a matter of debate because aquatic vertebrates have an abundant supply of calcium in freshwater and marine environments. As a consequence, it is likely that the skeleton would act only as an internal calcium source under conditions of mineral shortage. Instead, the post-cranial dermal skeleton (scales) would be more susceptible to resorption than the endoskeleton (62). Conversely, phosphate levels in water are generally low and unlikely to account for all body functions. Thus, the circulating concentration of phosphate depends on dietary P_i intake, intestinal absorption, renal filtration/secretion and reabsorption, and exchange from intracellular and bone reservoirs. For this reason, fish face mineral challenges different from those of terrestrial vertebrates with respect to the availability of these 2 elements (65, 66). In conditions of severe phosphate shortage (*e.g.*, low P_i dietary availability or systemic P_i homeostasis disorder), fish would need expeditious mobilization of phosphate ions to ensure the survival. Under these circumstances, the scales and endoskeleton would be the faster and more accessible sources for phosphate mobilization (Fig. 9*B*). In this context, ancient Pth4 would act in bone to promote phosphate mobilization and consequently mobilization of calcium. Our findings suggest a prominent role for Pth4 in maintenance of systemic phosphate homeostasis *via* control of bone mineral content, the major reservoir for calcium and phosphate. We cannot, however, exclude potential actions of Pth4 in gills and in intestinal reabsorption of phosphate through epithelia. During the vertebrate transition from the aquatic to terrestrial life, the parathyroid glands arose *via* transformation of the gills (67), with PTH1 emerging as the endogenous master regulator of bone mineral homeostasis. We hypothesize that during evolution of tetrapods, PTH1 gradually became the principal regulator of the calcium/phosphate metabolism and Pth4 was then lost in the eutherian vertebrates caused by redundancy. Our findings illustrate, therefore, the relevance of the identification of gene loss events to better understand the evolution and diversification of animal lineages (68). FJ

ACKNOWLEDGMENTS

The authors thank Yi-lin Yan (University of Oregon) for providing the *tip39* (*PTH2*) expression vector; Prof. N. Lawson (University of Massachusetts Medical School, Worcester, MA, USA) and Prof. K. Kawakami (National Institute of Genetics, Mishima, Japan) for providing the iTol2 constructs; D.A.P. for the hcrt:tdTomato line and Prof. K. M. Kwan (University Of Utah, Salt Lake City, UT, USA) for the bactin2:H2A-mCherry line; Inés Pazos and Jesús Méndez [Scientific and Technological Research Assistance Centre (CACTI), University of Vigo] for their advice and assistance with the confocal microscope; Rubén Chamorro and Rosa Ceinos (IIM–CSIC) for their help in handling and care of the fish and David Guede and José R. Caeiro (University of Santiago de Compostela, Santiago, Spain) for their advice and assistance with the micro-CT SkyScan. This work was funded by the Spanish Economy and Competitiveness Ministry Project ALG2011-23581 and AGL2014-52473R (to J.R.); the Portuguese Foundation for Science and Technology (Project PTDC/BIA-ANM/4225/2012-phos-fate; to P.G.); U. S. National Institutes of Health/Office of the Director Grant R01OD011116 (alias R01 RR020833; to J.H.P.); Generalitat de Catalunya (Grant SGR2014-290) and the Spanish Economy and Competitiveness Ministry (Project BFU2010-14875; to C.C.). Partial funding was

obtained from Science and Innovation Ministry (AGL2010-22247-C03-01; to J.M.C.-R.), a Campus do Mar Ph.D. grant, and Xunta de Galicia (Santiago, Spain; Project AGL2014-52473R) (to P.S.B.). C.C. and J.R. are co-senior authors.

AUTHOR CONTRIBUTIONS

J. Rotllant and P. Suarez-Bregua conceived, designed, and coordinated the study; C. Cañestro, I. Braasch, and J. H. Postlethwait performed comparative genomics analyses; P. Suarez-Bregua and E. Torres-Nuñez performed promoter and mutation analysis; J. Rotllant performed transgenic lines creation and screening with support from P. Suarez-Bregua and E. Torres-Nuñez; J. Cerda-Reverter and P. Suarez-Bregua performed receptor binding studies; P. Suarez-Bregua, A. Saxena, and M. E. Bronner performed laser ablation studies; P. Moran, D. A. Prober, P. Guerreiro, D. M. Power, S. J. Du, F. Adrio, D. M. Power, and A. V. M. Canario provided technical support and contributed to methodology; and P. Suarez-Bregua, C. Cañestro, and J. Rotllant wrote and revised the manuscript with input from A. Saxena, J. H. Postlethwait, and M. E. Bronner.

REFERENCES

1. Huitema, L. F., Apschner, A., Logister, I., Spoorendonk, K. M., Bussmann, J., Hammond, C. L., and Schulte-Merker, S. (2012) Entpd5 is essential for skeletal mineralization and regulates phosphate homeostasis in zebrafish. *Proc. Natl. Acad. Sci. USA* **109**, 21372–21377
2. Lu, Y., and Feng, J. Q. (2011) FGF23 in skeletal modeling and remodeling. *Curr. Osteoporos. Rep.* **9**, 103–108
3. Blair, H. C., Zaidi, M., Huang, C. L.-H., and Sun, L. (2008) The developmental basis of skeletal cell differentiation and the molecular basis of major skeletal defects. *Biol. Rev. Camb. Philos. Soc.* **83**, 401–415
4. Driessler, F., and Baldock, P. A. (2010) Hypothalamic regulation of bone. *J. Mol. Endocrinol.* **45**, 175–181
5. Elefteriou, F. (2008) Regulation of bone remodeling by the central and peripheral nervous system. *Arch. Biochem. Biophys.* **473**, 231–236
6. Quiros-Gonzalez, I., and Yadav, V. K. (2014) Central genes, pathways and modules that regulate bone mass. *Arch. Biochem. Biophys.* **561**, 130–136
7. Bajayo, A., Bar, A., Denes, A., Bachar, M., Kram, V., Attar-Namdar, M., Zallone, A., Kovács, K. J., Yirmiya, R., and Bab, I. (2012) Skeletal parasympathetic innervation communicates central IL-1 signals regulating bone mass accrual. *Proc. Natl. Acad. Sci. USA* **109**, 15455–15460
8. Kronenberg, H. M., Lanske, B., Kovacs, C. S., Chung, U. I., Lee, K., Segre, G. V., Schipani, E., and Jüppner, H. (1998) Functional analysis of the PTH/PTHrP network of ligands and receptors. *Recent Prog. Horm. Res.* **53**, 283–301, discussion 301–303
9. Potts, J. T. (2005) Parathyroid hormone: past and present. *J. Endocrinol.* **187**, 311–325
10. Guerreiro, P. M., Renfro, J. L., Power, D. M., and Canario, A. V. M. (2007) The parathyroid hormone family of peptides: structure, tissue distribution, regulation, and potential functional roles in calcium and phosphate balance in fish. *Am. J. Physiol. Regul. Integr. Comp. Physiol.* **292**, R679–R696
11. Pinheiro, P. L. C., Cardoso, J. C. R., Gomes, A. S., Fuentes, J., Power, D. M., and Canário, A. V. M. (2010) Gene structure, transcripts and calciotropic effects of the PTH family of peptides in Xenopus and chicken. *BMC Evol. Biol.* **10**, 373–387
12. Canario, A. V. M., Rotllant, J., Fuentes, J., Guerreiro, P. M., Rita Teodósio, H., Power, D. M., and Clark, M. S. (2006) Novel bioactive parathyroid hormone and related peptides in teleost fish. *FEBS Lett.* **580**, 291–299
13. Westerfield, M. (2007) The Zebrafish Book. A Guide for the Laboratory Use of Zebrafish (Danio rerio), University of Oregon Press, Eugene, OR
14. Kimmel, C. B., Ballard, W. W., Kimmel, S. R., Ullmann, B., and Schilling, T. F. (1995) Stages of embryonic development of the zebrafish. *Dev. Dyn.* **203**, 253–310
15. Guindon, S., Dufayard, J.-F., Lefort, V., Anisimova, M., Hordijk, W., and Gascuel, O. (2010) New algorithms and methods to estimate maximum-likelihood phylogenies: assessing the performance of PhyML 3.0. *Syst. Biol.* **59**, 307–321
16. Catchen, J. M., Conery, J. S., and Postlethwait, J. H. (2009) Automated identification of conserved synteny after whole-genome duplication. *Genome Res.* **19**, 1497–1505
17. Wolfe, K. (2000) Robustness: it's not where you think it is. *Nat. Genet.* **25**, 3–4
18. Cañestro, C., Catchen, J. M., Rodríguez-Marí, A., Yokoi, H., and Postlethwait, J. H. (2009) Consequences of lineage-specific gene loss on functional evolution of surviving paralogs: ALDH1A and retinoic acid signaling in vertebrate genomes. *PLoS Genet.* **5**, e1000496
19. Catchen, J. M., Braasch, I., and Postlethwait, J. H. (2011) Conserved synteny and the zebrafish genome. *Methods Cell Biol.* **104**, 259–285
20. Pfaffl, M. W. (2001) A new mathematical model for relative quantification in real-time RT-PCR. *Nucleic Acids Res.* **29**, e45
21. Rotllant, J., Liu, D., Yan, Y. L., Postlethwait, J. H., Westerfield, M., and Du, S. J. (2008) Sparc (Osteonectin) functions in morphogenesis of the pharyngeal skeleton and inner ear. *Matrix Biol.* **27**, 561–572
22. Cerdá-Reverter, J. M., Martínez-Rodríguez, G., Anglade, I., Kah, O., and Zanuy, S. (2000) Peptide YY (PYY) and fish pancreatic peptide Y (PY) expression in the brain of the sea bass (Dicentrarchus labrax) as revealed by ISH. *J. Comp. Neurol.* **426**, 197–208
23. Rubin, D. A., Hellman, P., Zon, L. I., Lobb, C. J., Bergwitz, C., and Jüppner, H. (1999) A G protein-coupled receptor from zebrafish is activated by human parathyroid hormone and not by human or teleost parathyroid hormone-related peptide: implications for the evolutionary conservation of calcium-regulating peptide hormones. *J. Biol. Chem.* **274**, 23035–23042
24. Sánchez, E., Rubio, V. C., and Cerdá-Reverter, J. M. (2009) Characterization of the sea bass melanocortin 5 receptor: a putative role in hepatic lipid metabolism. *J. Exp. Biol.* **212**, 3901–3910
25. Hoare, S. R., Rubin, D. A., Jüppner, H., and Usdin, T. B. (2000) Evaluating the ligand specificity of zebrafish parathyroid hormone (PTH) receptors: comparison of PTH, PTH-related protein, and tuberoinfundibular peptide of 39 residues. *Endocrinology* **141**, 3080–3086
26. Sánchez, E., Rubio, V. C., Thompson, D., Metz, J., Flik, G., Millhauser, G. L., and Cerdá-Reverter, J. M. (2009) Phosphodiesterase inhibitor-dependent inverse agonism of agouti-related protein on melanocortin 4 receptor in sea bass (Dicentrarchus labrax). *Am. J. Physiol. Regul. Integr. Comp. Physiol.* **296**, R1293–R1306
27. Chen, W., Shields, T. S., Stork, P. J. S., and Cone, R. D. (1995) A colorimetric assay for measuring activation of Gs- and Gq-coupled signaling pathways. *Anal. Biochem.* **226**, 349–354
28. Kawakami, K. (2007) Tol2: a versatile gene transfer vector in vertebrates. *Genome Biol.* **8**, S7.1–S7.10
29. Cartharius, K., Frech, K., Grote, K., Klocke, B., Haltmeier, M., Klingenhoff, A., Frisch, M., Bayerlein, M., and Werner, T. (2005) MatInspector and beyond: promoter analysis based on transcription factor binding sites. *Bioinformatics* **21**, 2933–2942
30. Wang, J., and Wilkinson, M. F. (2001) Deletion mutagenesis of large (12-kb) plasmids by a one-step PCR protocol. *Biotechniques* **31**, 722–724
31. Flores, M. V., Lam, E. Y. N., Crosier, P., and Crosier, K. (2006) A hierarchy of Runx transcription factors modulate the onset of chondrogenesis in craniofacial endochondral bones in zebrafish. *Dev. Dyn.* **235**, 3166–3176
32. Kalev-Zylinska, M. L., Horsfield, J. A., Flores, M. V., Postlethwait, J. H., Chau, J. Y., Cattin, P. M., Vitas, M. R., Crosier, P. S., and Crosier, K. E. (2003) Runx3 is required for hematopoietic development in zebrafish. *Dev. Dyn.* **228**, 323–336
33. Robu, M. E., Larson, J. D., Nasevicius, A., Beiraghi, S., Brenner, C., Farber, S. A., and Ekker, S. C. (2007) p53 activation by knockdown technologies. *PLoS Genet.* **3**, e78
34. Saxena, A., Peng, B. N., and Bronner, M. E. (2013) Sox10-dependent neural crest origin of olfactory microvillous neurons in zebrafish. *eLife* **2**, e00336
35. Feldkamp, L. A., Davis, L. C., and Kress, J. W. (1984) Practical cone-beam algorithm. *J. Opt. Soc. Am. A* **1**, 612–619
36. On, J. S. W., Duan, C., Chow, B. K. C., and Lee, L. T. O. (2015) Functional pairing of class B1 ligand-GPCR in cephalochordate provides evidence of the origin of PTH and PACAP/glucagon receptor family. *Mol. Biol. Evol.* **32**, 2048–2059

37. Yan, Y.-L., Bhattacharya, P., He, X. J., Ponugoti, B., Marquardt, B., Layman, J., Grunloh, M., Postlethwait, J. H., and Rubin, D. A. (2012) Duplicated zebrafish co-orthologs of parathyroid hormone-related peptide (PTHrP, Pthlh) play different roles in craniofacial skeletogenesis. *J. Endocrinol.* **214**, 421–435
38. Dehal, P., and Boore, J. L. (2005) Two rounds of whole genome duplication in the ancestral vertebrate. *PLoS Biol.* **3**, e314
39. Putnam, N. H., Butts, T., Ferrier, D. E. K., Furlong, R. F., Hellsten, U., Kawashima, T., Robinson-Rechavi, M., Shoguchi, E., Terry, A., Yu, J.-K., Benito-Gutiérrez, E. L., Dubchak, I., Garcia-Fernàndez, J., Gibson-Brown, J. J., Grigoriev, I. V., Horton, A. C., de Jong, P. J., Jurka, J., Kapitonov, V. V., Kohara, Y., Kuroki, Y., Lindquist, E., Lucas, S., Osoegawa, K., Pennacchio, L. A., Salamov, A. A., Satou, Y., Sauka-Spengler, T., Schmutz, J., Shin-I, T., Toyoda, A., Bronner-Fraser, M., Fujiyama, A., Holland, L. Z., Holland, P. W. H., Satoh, N., and Rokhsar, D. S. (2008) The amphioxus genome and the evolution of the chordate karyotype. *Nature* **453**, 1064–1071
40. Cañestro, C. (2012) Two rounds of whole-genome duplication: evidence and impact on the evolution of vertebrate innovations. In *Polyploidy and Genome Evolution* (Soltis, P., and Soltis, D. E., eds.), Springer-Verlag, Berlin, p. 309–339 doi:10.1007/978-3-642-31442-1_16
41. Li, N., Felber, K., Elks, P., Croucher, P., and Roehl, H. H. (2009) Tracking gene expression during zebrafish osteoblast differentiation. *Dev. Dyn.* **238**, 459–466
42. van der Velden, Y. U., Wang, L., Querol Cano, L., and Haramis, A.-P. G. (2013) The polycomb group protein ring1b/rnf2 is specifically required for craniofacial development. *PLoS One* **8**, e73997
43. Gardella, T. J., and Jüppner, H. (2001) Molecular properties of the PTH/PTHrP receptor. *Trends Endocrinol. Metab.* **12**, 210–217
44. Hori, M., Shimizu, Y., and Fukumoto, S. (2011) Minireview: fibroblast growth factor 23 in phosphate homeostasis and bone metabolism. *Endocrinology* **152**, 4–10
45. Bhattacharya, P., Yan, Y. L., Postlethwait, J., and Rubin, D. A. (2011) Evolution of the vertebrate pth2 (tip39) gene family and the regulation of PTH type 2 receptor (pth2r) and its endogenous ligand pth2 by hedgehog signaling in zebrafish development. *J. Endocrinol.* **211**, 187–200
46. Hoshi, K., Komori, T., and Ozawa, H. (1999) Morphological characterization of skeletal cells in Cbfa1-deficient mice. *Bone* **25**, 639–651
47. Zheng, Q., Zhou, G., Morello, R., Chen, Y., Garcia-Rojas, X., and Lee, B. (2003) Type X collagen gene regulation by Runx2 contributes directly to its hypertrophic chondrocyte-specific expression in vivo. *J. Cell Biol.* **162**, 833–842
48. Nishio, Y., Dong, Y., Paris, M., O'Keefe, R. J., Schwarz, E. M., and Drissi, H. (2006) Runx2-mediated regulation of the zinc finger Osterix/Sp7 gene. *Gene* **372**, 62–70
49. Gensure, R. C., Ponugoti, B., Gunes, Y., Papasani, M. R., Lanske, B., Bastepe, M., Rubin, D. A., and Jüppner, H. (2004) Identification and characterization of two parathyroid hormone-like molecules in zebrafish. *Endocrinology* **145**, 1634–1639
50. Suzuki, N., Danks, J. A., Maruyama, Y., Ikegame, M., Sasayama, Y., Hattori, A., Nakamura, M., Tabata, M. J., Yamamoto, T., Furuya, R., Saijoh, K., Mishima, H., Srivastav, A. K., Furusawa, Y., Kondo, T., Tabuchi, Y., Takasaki, I., Chowdhury, V. S., Hayakawa, K., and Martin, T. J. (2011) Parathyroid hormone 1 (1-34) acts on the scales and involves calcium metabolism in goldfish. *Bone* **48**, 1186–1193
51. Rotllant, J., Guerreiro, P. M., Redruello, B., Fernandes, H., Apolónia, L., Anjos, L., Canario, A. V. M., and Power, D. M. (2006) Ligand binding and signalling pathways of PTH receptors in sea bream (Sparus auratus) enterocytes. *Cell Tissue Res.* **323**, 333–341
52. Anjos, L., Gomes, A. S., Redruello, B., Reinhardt, R., Canário, A. V., and Power, D. M. (2013) PTHrP-induced modifications of the sea bream (Sparus auratus) vertebral bone proteome. *Gen. Comp. Endocrinol.* **191**, 102–112
53. Guerreiro, P. M., Canario, A. V. M., Power, D. M., and Renfro, J. L. (2010) Piscine PTHrP regulation of calcium and phosphate transport in winter flounder renal proximal tubule primary cultures. *Am. J. Physiol. Regul. Integr. Comp. Physiol.* **299**, R603–R611
54. Martin, A., David, V., and Quarles, L. D. (2012) Regulation and function of the FGF23/klotho endocrine pathways. *Physiol. Rev.* **92**, 131–155
55. Radanovic, T., Wagner, C. A., Murer, H., and Biber, J. (2005) Regulation of intestinal phosphate transport, I: segmental expression and adaptation to low-P(i) diet of the type IIb Na(+)-P(i) cotransporter in mouse small intestine. *Am. J. Physiol. Gastrointest. Liver Physiol.* **288**, G496–G500
56. Graham, C., Nalbant, P., Schölermann, B., Hentschel, H., Kinne, R. K. H., and Werner, A. (2003) Characterization of a type IIb sodium-phosphate cotransporter from zebrafish (Danio rerio) kidney. *Am. J. Physiol. Renal Physiol.* **284**, F727–F736
57. Yadav, M. C., Simão, A. M. S., Narisawa, S., Huesa, C., McKee, M. D., Farquharson, C., and Millán, J. L. (2011) Loss of skeletal mineralization by the simultaneous ablation of PHOSPHO1 and alkaline phosphatase function: a unified model of the mechanisms of initiation of skeletal calcification. *J. Bone Miner. Res.* **26**, 286–297
58. Christov, M., and Jüppner, H. (2013) Insights from genetic disorders of phosphate homeostasis. *Semin. Nephrol.* **33**, 143–157
59. Tseng, D. Y., Chou, M. Y., Tseng, Y. C., Hsiao, C. D., Huang, C. J., Kaneko, T., and Hwang, P. P. (2009) Effects of stanniocalcin 1 on calcium uptake in zebrafish (Danio rerio) embryo. *Am. J. Physiol. Regul. Integr. Comp. Physiol.* **296**, R549–R557
60. Khanal, R. C., and Nemere, I. (2008) Endocrine regulation of calcium transport in epithelia. *Clin. Exp. Pharmacol. Physiol.* **35**, 1277–1287
61. Abbink, W., Bevelander, G. S., Hang, X., Lu, W., Guerreiro, P. M., Spanings, T., Canario, A. V. M., and Flik, G. (2006) PTHrP regulation and calcium balance in sea bream (Sparus auratus L.) under calcium constraint. *J. Exp. Biol.* **209**, 3550–3557
62. Rotllant, J., Redruello, B., Guerreiro, P. M., Fernandes, H., Canario, A. V., and Power, D. M. (2005) Calcium mobilization from fish scales is mediated by parathyroid hormone related protein via the parathyroid hormone type 1 receptor. *Regul. Pept.* **132**, 33–40
63. Galitzer, H., Ben-Dov, I., Lavi-Moshayoff, V., Naveh-Many, T., and Silver, J. (2008) Fibroblast growth factor 23 acts on the parathyroid to decrease parathyroid hormone secretion. *Curr. Opin. Nephrol. Hypertens.* **17**, 363–367
64. Penido, M. G. M. G., and Alon, U. S. (2012) Phosphate homeostasis and its role in bone health. *Pediatr. Nephrol.* **27**, 2039–2048
65. Lewis-McCrea, L. M., and Lall, S. P. (2010) Effects of phosphorus and vitamin C deficiency, vitamin A toxicity, and lipid peroxidation on skeletal abnormalities in Atlantic halibut (Hippoglossus hippoglossus). *J. Appl. Ichthyol.* **26**, 334–343
66. Witten, P. E., and Huysseune, A. (2009) A comparative view on mechanisms and functions of skeletal remodelling in teleost fish, with special emphasis on osteoclasts and their function. *Biol. Rev. Camb. Philos. Soc.* **84**, 315–346
67. Okabe, M., and Graham, A. (2004) The origin of the parathyroid gland. *Proc. Natl. Acad. Sci. USA* **101**, 17716–17719
68. Albalat, R., and Cañestro, C. (2016) Evolution by gene loss. *Nat. Rev. Genet.* **17**, 379–391

Received for publication July 27, 2016.
Accepted for publication October 11, 2016.